Recent Technique Developments and Applications of Solid State NMR in Characterising Inorganic Materials

J. V. Hanna and M. E. Smith*

Department of Physics, University of Warwick, Coventry, UK, CV4 7AL

Abstract

A broad overview is given of some key recent developments in solid state NMR techniques that have driven enhanced applications to inorganic materials science. Reference is made to advances in hardware, pulse sequences and associated computational methods (e.g. first principles calculations, spectral simulation), along with their combination to provide more information about solid phases. The resulting methodology has allowed more nuclei to be observed and more structural information to be extracted. Cross referencing between experimental parameters and their calculation from the structure has seen an added dimension to NMR as a characterisation probe of materials. Emphasis is placed on the progress made in the last decade especially from those nuclei that were little studied previously. The general points about technique development and the increased range of nuclei observed are illustrated through a range of specific exemplars from inorganic materials science.

* Author for correspondence: M.E. Smith, Department of Physics, University of Warwick, Coventry, UK, CV4 7AL
Email M.E.Smith.1@warwick.ac.uk

1. Introduction

The exact starting point of a specific area of scientific endeavour can often be difficult to pin point. The application of high resolution solid state NMR to inorganic materials is probably no different, but the collaboration in the late 1970s between Engelhardt and the Tallinn Group showing that Q^n species in solid silicates could be distinguished on the basis of the ^{29}Si chemical shift under MAS was a pivotal moment [e.g. 1]. The book by Engelhardt and Michel provides an excellent overview of development in that period [2]. Since then there has been a rapid expansion in the capability and use of solid state NMR and a comprehensive snapshot of the background and development of the technique in its application to inorganic materials until up to mid-2001 is provided by ref. 3. This Trends article aims to capture some of the new aspects of solid state NMR applied to inorganic materials since that point as the intervening decade has seen some further exciting, major developments in the field. The article is intended to be accessible to the non-expert, who has some background knowledge of, and is a solid state NMR user wanting to increase the use of the technique in his/her research. A number of key aspects of the technique that are to a certain extent taken for granted in 2010 were far from so a decade ago. This article examines some of those key developments, such as in hardware where for example high magnetic fields (i.e. > 14.1 T) and fast MAS (> 35 kHz) have become much more widely available, as have pulse methods built on the high resolution MQ work of Frydman [4]. Pulsed methods with increasing sophistication to extract structural information have been developed, which exploit the fact that in solids the local J-coupling and dipolar couplings are preserved. The short-range nature of the NMR interactions means that solids which lack long-range order (e.g. amorphous, atomically disordered crystalline systems) are amenable to investigation. A huge change in the last decade has been the ability to calculate NMR interactions from the structure, via for example DFT, and hence there is a new level of sophistication available to constrain structure from the determination of NMR interactions. To illustrate the progress that has been made the applications part is split into looking at nuclei and some exemplar materials systems that are of much contemporary interest, especially where there is much more activity than a decade ago. To make the scope of the article more manageable a clear focus is placed on examples where the NMR has been applied to simple inorganic solids (as opposed to for example organometallics where there is an increasingly rich literature) or to a key inorganic materials science problem. Where possible, reference is made to recent review articles to provide more details of a specific area.

2. Development of Techniques Applicable to Solid State NMR of Inorganic Materials

2.1 Hardware

In any NMR experiment two of the key factors are the magnetic field and the probe chosen. The availability in the mid-1990s of wide bore (89 mm) 14.1 T instruments made a huge difference to the quality of spectra from a number of key nuclei such as ^{23}Na and ^{27}Al, as second-order quadrupolar effects were better suppressed because of their inverse applied magnetic field (B_o) dependence [3, 5, 6]. Higher magnetic fields also increased sensitivity, such that NMR studies of inorganic materials using insensitive nuclei, such as ^{17}O became more popular [7]. These advantages increased still further as persistent fields of ≥ 20 T became more widely available, with currently the state of the art corresponding to wide bore 20 T commercial instruments, with a few higher field facilities for solids equipped with 21.1 and 23.5 T instruments, but with standard bore (57 mm) magnets. The other point about the wider availability of particularly high field magnets and appropriate MAS probes is the variable field approach to determining quadrupolar interaction parameters [3, 8] becoming more widely used. The differing field dependencies of the second-order quadrupolar interaction ($\propto B_o^{-1}$, in Hz) and chemical shift interaction ($\propto B_o$, in Hz) means that measurements at two fields, with three or more preferred, much better constrain the NMR interactions determined. If the CSA, which is averaged by MAS, also needs to be determined then a combination of static and MAS measurements at differing magnetic fields is necessary. Two practical examples are shown in Fig. 1. ^{25}Mg MAS at three magnetic fields (11.7, 14.1 and 18.8 T) is used to constrain and determine the isotropic chemical shift (δ_{iso}), the quadrupolar coupling constant (χ_Q,) and quadrupolar asymmetry parameter (η_Q, see refs 3, 5 for definition of these parameters) in $MgSO_4.6H_2O$ [9]. Despite the strong overlap between these two sites the NMR parameters are well constrained by this approach. An example where CSA is also present is the ^{93}Nb NMR spectra of $YNbO_4$ where although there is clearly a large second-order quadrupole interaction, there is also significant CSA. Again data collected at multiple fields (here four) strongly constrains the interactions [10]. Work on constraining the NMR interaction parameters has also been pushed forward even for much studied nuclei such as ^{23}Na and ^{27}Al. MQ MAS techniques are now well established for resolving overlapping lineshapes from such nuclei. The retention of second-order quadrupolar and isotropic information in the different dimensions of the 2D data sets can also help separate the different NMR interaction parameters. This approach can also be used in combination with multiple field 1D data sets, including iteratively, to constrain a quantitative fit of the 1D MAS lineshape (see section 2.5.1).

Another key variable in determining the practical limitations that MAS can be applied to is the maximum MAS rate. The increase in the maximum spinning speed has followed the decrease

in diameters of the rotors available, with key steps being 5 kHz (7/7.5 mm), 15 kHz (4 mm), 25 kHz (3.2 mm) and 35 kHz (2.5 mm) by the mid-1990s. Increasing rotor speed has meant fewer spinning sidebands (although the anisotropic information conveyed by can be important) producing cleaner spectra and better S/N for the same amount of sample, as well as larger ranges of interactions, especially dipolar and quadrupolar are able to be averaged to give the best possible resolution. Faster MAS has also meant that paramagnetic systems become more tractable to high resolution techniques (Sec 4.3). The major change in the last decade has been to even smaller diameter rotors of 2, 1.5 and now even 1 mm. Currently the smallest diameter rotors commercially available are 1.3 mm which provide upper spinning speeds of ~70 kHz. Some non-commercial prototypes have reported maximum spinning speeds of 90 kHz. Smaller rotors provide better mass-sensitivity such that samples with limited availability become more tractable, which although not often a limitation for many inorganic materials problems, for some cases with isotopic enrichment can be useful. As spinning speeds in excess of 50 kHz have been reached many of the typical spin interactions were exceeded. High resolution proton spectroscopy from solids has been a long-standing problem as the strong dipolar interacting spins make the linewidth homogeneous, which cannot be refocused periodically. Nevertheless, fast MAS brings a considerable improvement in resolution. While experimental results show that proton linewidths decrease only linearly with the rotor speed, the effect is more pronounced in 2D spectra where the diagonal separation of resonances is improved by an additional factor of $\sqrt{2}$ [11]. Fast MAS increasing the utility of proton NMR is more relevant to organic materials since in inorganic materials the proton density is usually low enough that even modest MAS rates (e.g. 25 kHz) can be sufficient. Another key point is that in complex pulse sequences that combine spatial reorientation with spin manipulation (e.g. decoupling, coherent spin motion, etc.) via rf pulses it has always been assumed that the MAS rate is the slow motion. With such high MAS rates this is no longer necessarily true. This opens up new possibilities for the manipulation of the spins.

A variation for small samples is to use microcoils which are not necessarily to provide ultrafast MAS since a number of the designs piggyback the sample container onto a conventional small MAS rotor. A whole range of careful considerations are necessary to ensure that sensitivity is maximised from small samples and that the small coils do not cause loss of resolution through susceptibility broadening nor rf inhomogeneity. Several different coils have been suggested for such systems including solenoids, flat helices and stripline/microslot designs which have been compared [12]. An additional advantage is that tremendously high rf fields can be generated which makes direct observation of some very broad NMR lines possible. As an example (Fig. 2) the spin-echo spectrum of α-Al_2O_3 powder with χ_Q = 2.4 MHz is shown, which in a normal diameter

solenoid probe would be very difficult to record because of the limited rf available relative to the linewidth. With a 300 μm coil and 850 W of power, an rf field of 3 MHz can be produced. These conditions allow spectra extending over 1 MHz to be recorded [13]. The stripline solution produces spatially localised rf fields such that NMR of thin films can be realised, which could find several potentially important applications in inorganic materials science, such as for surface layers. An alternative strategy using inductive coupling enabling wireless transmission of the rf pulses and detection of the signal from the sample under fast MAS also holds a lot of promise [14]. Although still not widely available the specific advantages offered by such microcoils should see more application in the area of inorganic materials in the future.

DOR was introduced as a technique in around 1988 [15] as a direct 1D approach to provide high resolution spectra from second-order quadrupolar broadened nuclei. The DOR solution used the mechanical sophistication of a 'rotor within a rotor' system such that the sample is simultaneously spun around the magic angles for both the second-order (54.74º) and fourth-order Legendre polynomials (30.56º and 70.15º, with the smaller angle chosen for practical reasons). The concept is very neat, but did not catch on because of the relatively low spinning speed of the outer rotor (~ 1 kHz, which produced many spinning sidebands), the lack of long term spinning stability and the need for a specialised probe. It remains the only technique that gives high resolution spectra from quadrupole nuclei in real time in a directly analogous way to MAS. There has recently been renewed interest in the application of DOR NMR, which has been catalysed by developments of DOR probe heads, with smaller outer rotors allowing faster spinning (up to ~ 2 kHz) and probably most importantly the long term stability offered by computer controlled air pressures. This new generation of probes then allows concepts beyond just simply distinguishing sites on the basis of improved resolution to be introduced, providing additional structural information via the quantitative determination of anisotropic interactions. Examples of such experiments have been to use the sideband pattern intensity to detect dipolar coupling and CSA, as well as their relative orientations [16]. As an example the ^{17}O NMR spectrum of L-alanine (Fig. 3) shows that the sideband intensity cannot be reproduced by simply including the quadrupolar interaction, but has to include CSA as well, which can then be accurately determined. Hence DOR should be seriously considered in the specialised solid state NMR armoury for characterising materials.

2.2 New High Resolution Methods for Quadrupolar Nuclei

Improving resolution remains a challenge for solid state NMR of quadrupolar nuclei. Combining and extending techniques is one approach for improving resolution, with MQDOR

being such an example [17, 18]. MQDOR spectra can be transformed via shear and scaling transformations to give a 2D representation in which the F_1 and F_2 frequencies correspond to the isotropic second-order quadrupolar shift and chemical shift, respectively, with the protocol for such a transformation having been presented for all spins and differing MQ coherence order [18]. In measuring $RbNO_3$ using this approach very narrow resonances were obtained with the linewidths solely being determined by homogeneous effects to produce values for ^{87}Rb of ~0.1 and 0.2 ppm in the quadrupolar and chemical shift dimensions, enabling the highly accurate determination of the isotropic chemical shift and the combined quadrupolar product, P_Q. For amorphous materials the use of MQDOR to remove line broadening interactions allows the chemical shift and EFG distributions to be directly determined which is difficult from other approaches such as multiple field analysis of MAS and/or MQ data since the interactions are convoluted in a single parameter. After shearing and scaling the two projections, isotropic chemical shift and quadrupolar interaction distributions which are completely independent of each other are obtained which has been applied to vitreous B_2O_3 [18]. An interesting comparison of 1D MAS, DOR, 3Q and 5Q MAS was made for ^{27}Al by taking data from two much studied compounds $AlPO_4$-14 and andalusite, a polymorph of Al_2SiO_5. The need for strong rf excitation to provide the best sensitivity for 5Q experiments was clear. The 1D techniques were much more sensitive in terms of the S/N produced in a fixed time [19], and DOR has good sensitivity despite the relatively poor filling factor.

While the MQ MAS experiment has been very successful other variants have been demonstrated with ST MAS an alternative MAS-based correlation method [20, 21]. The correlation in this case is between the CT and the satellites via single quantum states which offers significant sensitivity advantages over MQ transitions. The first-order quadrupolar broadening of the satellite transitions means that the experiment must be rotor-synchronized in order to ensure the complete removal of this interaction. Hence although the experiment can be performed with a conventional probe head it does place considerable technical demands, such as very precise setting of the magic angle (to within ±0.002°), very accurate pulse timings and stable sample spinning [22]. In many commercial probes this made the experiment a bit hit and miss, but more probes that meet the stringent requirements have become available. The approach has shown real advantages when resolution is required, but sensitivity is an issue, such as is experienced in the cases of nuclei with small magnetic moments or where a very limited amount of sample is available. A good illustration of this is ^{17}O NMR of high pressure magnesium silicate phases [23]. STMAS, like MQMAS is still a 2D experiment and not a real time (e.g. like DOR) experiment. Various other experiments have been proposed to effectively acquire high resolution data from quadrupolar

broadened spectra. For I = 3/2 nuclei Wimperis introduced an experiment [24] for acquiring isotropic NMR spectra in real time, termed STARTMAS. This experiment requires very accurate timing of a series of rotor-synchronised pulses to interconvert ST and DQ transitions throughout acquisition, with the ratio of evolution times chosen such that the quadrupolar broadening is refocused. Another method based on the standard STMAS approach initiated the experiment via a series of selective pulses applied at different frequency offsets that create a series of echoes in the conventional acquisition, from which a 2D spectrum can be formed [25]. Both these experiments are highly innovative and effectively allow acquisition of both 2D and isotropic spectra using a single scan. The question of the impact these will have on the study of inorganic materials, especially compared to DOR will be interesting to follow in the next few years.

2.3 Methods for Improving Sensitivity and Wideline Observation from Quadrupolar Nuclei

With quadrupolar nuclei making up such a large fraction (~ 75%) of the NMR-active nuclei of the Periodic Table considerable effort has been undertaken to allow more efficient collection of undistorted spectra from broad lines and to enhance the signal of the observed transitions. To allow unambiguous simulation especially when multiple interactions are present, although distortions can be taken in account, collecting undistorted experimental spectra pays dividends. Using frequency offset techniques, such as VOCS, allow such spectra to be collected [26].

The QCPMG pulse sequence (Fig. 4(b)) consists of a train of selective π-pulses which refocus the magnetisation in the transverse plane allowing multiple spin-echoes to be recorded during each acquisition, thereby enhancing the amount of signal obtained in each scan which has been reviewed in detail [27, 28]. The last period of the pulse sequence is extended to ensure full acquisition of the free induction decay. Fourier transformation of the recorded echo train results in a spectrum consisting of narrow “spikelets”, whose widths are determined by the T_2 spin-spin relaxation time (*i.e.* the decay of the echo envelope) and whose separation in the frequency domain is the inverse of the echo separation in the time domain. The manifold of these spikelets represents the regular MAS lineshape that would be obtained by Fourier transformation of one half-echo. The gain in S/N comes from the concentration of the signal intensity into these narrow spikelets. The maximum possible enhancement will depend on the value of T_2 for the particular sample, since this determines how many echoes can be recorded in each scan. The QCPMG experiment is now widely exploited especially when sensitivity is a real issue, such as nuclei with small magnetic moments.

PT experiments involve the use of pulse sequences applied prior to the acquisition period which can enhance the NMR signal arising from the CT (which is the transition generally observed) of a half-integer spin quadrupolar nucleus by transferring polarisation from the ST. The NMR signal that arises from the CT is proportional to the population difference across the ±½ levels. If the STs can be saturated while the CT is left unaffected, this population difference can be increased by a factor of I + ½ for any half-integer spin quadrupolar nucleus of spin I. Such saturation of the STs can be achieved using the RAPT pulse sequence [29], a train of pulses with constant amplitude and alternating in phase (Fig. 4(a)), leading to a constant modulation frequency $\nu_{RAPT} = (2p+2t)^{-1}$. Maximum signal enhancement has been shown to occur when the RAPT loop duration is equal to one MAS rotor period and when $\nu_{RAPT} \approx \chi_Q/4$ where χ_Q is the quadrupolar coupling constant [29]. Even greater enhancement of the population difference across the CT can be obtained if the STs are inverted, rather than saturated, producing a factor 2I. One way in which the STs can be inverted without affecting the CT is by applying adiabatic inversion pulses [30] to the STs. In CT signal enhancement experiments, adiabatic pulses are applied at an offset far from the CT frequency so as to only invert the STs. The enhanced CT signal can then be observed in the usual way using a CT-selective 90° pulse or a Hahn-echo sequence with CT-selective 90° and 180° pulses. Recently it has been shown that applying an adiabatic inversion to a single ST spinning sideband is enough to invert the entire ST manifold. Other adiabatic pulse shapes have also been proposed, including WURST [31] and DFS where the latter employs a constant-amplitude pulse whose frequency is swept adiabatically [32]. Since QCPMG only involves manipulation of the spins during the acquisition, it is also possible to apply PT sequences prior to the QCPMG pulse train to provide further signal enhancement [33]. A comparison for some of these sequences is shown for ^{33}S in Fig. 4(c). RAPT creates a significant signal enhancement from the direct echo and the further advantage of QCPMG is readily observed, which can in turn also get a signal boost from RAPT.

2.4 Correlation Experiments

The presence of interactions such as through bond scalar/J-coupling, or through space dipolar coupling gives more insight into structure than the direct 1D spectrum since these interactions convey information about direct covalent bonding (J) and hence connectivity, or spatial relations of different nuclei over the distance of a few bond lengths, i.e. medium-range order. Even though these interactions are very small, with for example the J-coupling not explicitly resolved, the coupling can modulate the signal and hence its effect be detected. The experiments usually rely on the magnetisation being attributable to specific sites nuclei which in

most cases means there needs to be spectral resolution. For this reason correlation experiments tend to be better developed for spin-½ nuclei. Experiments such as CP have long been used for example in silicates to distinguish differently protonated Q^n species [3]. The refocused INADEQUATE experiment (Figure 5(a)) exploits the internuclear J-coupling interaction to identify nuclear spins that are linked via chemical bonds. The refocused version uses an additional π-pulse to obtain in-phase correlations, making it applicable to the solid state, where linewidths tend to be much broader than in solution. 2D correlation sequences are well established for ^{31}P, utilising the high sensitivity of this nucleus, and can be used to identify which phosphorus sites are linked via bridging oxygens. In favourable cases it can also be used to measure phosphate chain lengths and identify the chemical shifts of each site in the chain in the correct sequence [34, 35]. In many cases precise values of distances are not required, as semi-quantitative estimates provide the necessary information. DQF homonuclear correlation spectra are suitable for detection of inter and intramolecular contacts. DQ coherence is excited by relatively simple sequences of orthogonal 90^o pulses at the beginning and end of every half rotor period. Reconversion of the homonuclear DQ coherence to a SQ coherence generates a spectrum that represents only the closest dipolar coupled spins. The 2D DQF spectrum can be used to correlate spin pairs and the packing environment for each spin can be elucidated. A practical materials example is shown in Fig. 5(b) where the ^{31}P DQ refocused INADEQUATE of a crystallised Na_2O-CaO-P_2O_5 glass is shown with 12 different ^{31}P peaks, some barely resolved due to their overlap and low intensity. X-ray diffraction identifies two crystalline products β-$Ca(PO_3)_2$ and $NaCa(PO_3)_3$ which can be assigned to the relevant ^{31}P resonances. However six lower intensity peaks remain unassigned and these are revealed to be part of a single chain. This is a good example of the complementarity of different physical probe techniques and how advanced NMR methods can provide new information. Such correlation methods (particularly homonuclear variants) are much less common for quadrupolar nuclei because of the usually poorer resolution from such nuclei, although if resolution can be regained then many of the same sequences can be applied. In heteronuclear correlation experiments if one of the nuclei involved is spin-½ this can be the detected nucleus.

The dipolar coupling is also usually weak and naturally averaged under MAS. However a series of pulse sequences have been developed that can reintroduce the interaction in sequences such as HMQC, HSQC and rotary resonance recoupling (R^3). As a through space interaction it means it only provides information on spatial proximity and not bonding. Indirect detection of coupling via INEPT of J-HMQC has allowed various connectivities in inorganic systems to be determined [36]. Correlation techniques for quadrupolar nuclei have been recently reviewed in Trends articles [37, 38]. Some examples of correlation experiments are given in some of the

applications examined below. Homonuclear dipolar recoupling has allowed DQ correlations to be observed in amorphous solids. A practical consideration in these systems is to increase the robustness of the sequences to spreads of frequency, as found in amorphous materials. In a lanthanum aluminate glass ($La_{0.18}Al_{0.82}O_{1.5}$) such correlation experiments have been applied to map the ^{27}Al-^{27}Al correlations. The structure has the expected AlO_4, AlO_5 and AlO_6, but these units are not all randomly mixed, with the dominant structural motifs the AlO_4 connected with AlO_4, AlO_5 and AlO_6, and no connections between the other units (e.g. AlO_5-AlO_6, etc.) [39].

2.5 Software and Computational Methods

The ability to analyse the data from NMR experiments and to calculate the expected NMR interactions parameters on the basis of structure has improved greatly over the last decade. This section is broken up into looking at packages for analysing the experimental data and then first principles calculations of NMR parameters.

2.5.1 Lineshape Analysis and Simulation of Experiments

Several computer programs currently exist for fitting solid state NMR spectra, and for taking into account the effects of the pulse sequences on lineshapes. In our own laboratory or in collaboration with others, a range of packages are used that include SIMPSON, WSolids, DMFit and recommend them all for different specific problems. We recently compared these programmes and added a spectral simulation programme of our own QuadFit [40]. QuadFit is tailored towards fitting of NMR spectra from amorphous materials, but is also equally applicable to spectra from crystalline materials (http://go.warwick.ac.uk/quadfit). DMFit is a program written by Massiot [41] which has basic processing capabilities and extensive fitting abilities for both 1D and 2D data. SIMPSON [42] has been developed to produce very accurate simulations of NMR spectra given a set of spins, their interactions and a pulse sequence using density matrix theory. WSolids [43] is a simulation program for NMR spectra rather than a fitting program.

In disordered samples, the sharp features of the second-order quadrupolar lineshapes (such as observed in Fig. 1) are often smoothed by distributions in the quadrupolar parameters (an effect that also distorts and broadens the horizontal ridges in the MQMAS spectrum, causing it to spread in the SQ dimension). Then in addition to the average values, distributions of the interaction parameters can be determined and again multiple B_o data may be simulated using, *e.g.*, a Gaussian distribution in χ_Q, which can provide at least a semi-quantitative measure of the extent of disorder in the system. As an example the ^{71}Ga MAS NMR spectra are shown (Fig. 6) for β-Ga_2O_3 from an annealed crystalline sample where a well defined second-order quadrupolar lineshape can be

observed [44]. Then as this sample is ball milled defects are introduced which cause a much larger spread of interaction parameters. The spectra were simulated with the same average quadrupolar interaction χ_Q = 8.34 MHz. However in the crystalline sample only a small spread of values $\Delta\chi_Q$ = 0.40±0.05 MHz was needed, whereas this has risen considerably in the ball-milled sample to $\Delta\chi_Q$ = 2.20±0.15 MHz. There have also been recent advances in the understanding of the distributions in the quadrupolar parameters from disordered solids. The Czjzek model for the distribution of the EFG tensor in disordered solids, results from the statistical rotational invariance of a disordered solid and from the applicability of a central limit theorem to the EFG tensor [45, 46]. The basic Czjzek model has recently been extended that effectively argues that starting from a well defined local environment (as would be the case for the β-Ga_2O_3 given above) with values of the asymmetry parameter and of the principal component V_{zz} of the EFG tensor, perturbed by the disorder caused by effects further from the local atoms. The effect of disorder is simulated by Gaussian 'noise' about these values [46], with the essence to provide a means to extract information about the local environment and hence the disorder present in the material. The combination of the 1D spectra (especially if constrained at several magnetic fields) and the 2D contours of MQ data can really constrain the interactions and their distribution. This has really brought about an advance in analysing disordered inorganic materials in recent years.

2.5.2 First Principles Calculations of NMR Parameters

The benefits of combining solid state NMR and first principles quantum mechanical calculations for structural elucidation are widely recognised. Calculation of the EFG is in principle the most straightforward of the NMR interactions (compared to e.g. the chemical shielding) as it only requires knowledge of the ground state charge density, the ground state wave function and the position of the atoms within the unit cell. Also it does not involve the calculation of any response of the system to B_o. Blaha and colleagues used a plane-wave method implemented as the WIEN code [47]. EFGs can also be calculated by *ab initio* DFT calculations using the GIPAW method (CASTEP code), an accurate (all electron) approach to solving the Kohn-Sham DFT equations, although its accuracy does come at a computational cost. In contrast, the recently introduced alternative GIPAW method uses a pseudopotential to distinguish core and valence states. This creates a smoother approximation to the wavefunction and reduces the number of plane waves required, thereby increasing the computational efficiency. This has been implemented as the CASTEP code [48, 49] which can also calculate the shielding as a linear response of the system to B_o. A very recent example specifically targeted at using such an approach for materials applications was to calculate the ^{17}O and ^{71}Ga NMR interaction parameters from a series of

relatively simple oxides and gallates. The agreement between the calculations and experiment for the most part was good, sufficient to encourage the use of this combined approach to provide real insight into the oxygen site coordination in doped systems that are candidates for intermediate solid oxide fuel cell electrolytes. It is noted that one of the sources of error is that the calculations rely on the motionally and spatially averaged structure determined by diffraction and not the local structure experienced on the NMR timescale. Approaches to incorporate such effects in calculations beyond pure DFT are challenging, but are a possible interesting future direction [50]. Other examples of how these methods can be used to help understand the structural implications of the measured NMR interaction parameters will be given below in some specific materials systems.

3. Progress in Observation of Less Studied Nuclei

In the past decade the bulk of solid state NMR studies have involved the well established nuclei. For inorganic materials key nuclei that fall into this category are ^{11}B, ^{23}Na, ^{27}Al, ^{29}Si and ^{31}P. Specific examples of extensions of applications of these nuclei to important materials science and technology problems are given in Section 4. The last decade has seen a significant increase in the range of nuclei observed (i.e. the approach has become more multinuclear). This section briefly looks at (i) examples of interesting new applications of less studied nuclei in inorganic materials, and (ii) draws attention to extensive new studies of such nuclei.

3.1 Spin-½ Nuclei

^{89}Y is a low-γ nucleus (with low usually defined as having a magnetic moment smaller than ^{15}N) [51], but good quality data has been obtained from $Y_2(Ti_{2-x}Sn_x)O_7$ solid solutions, with ^{89}Y's large chemical shift range ensuring good discrimination between the different local environments [52]. Distinct ^{89}Y resonances were seen for each different number of next nearest neighbour (nnn) B site tins. Using a purely statistical analysis, the relative probability (P) of each site (e.g. with *n* tin nnn on the B site) is $P(n\ \mathrm{Sn}) = \Omega\ p^n(1-p)^{6-n}$, where Ω is the number of permutations and p = x/2. From such an analysis, the experimental intensities very closely match that for a random distribution. This work was recently extended to use first principles DFT calculations. The shift values calculated and the effects of the Ti,Sn ordering confirmed that the yttrium does remain eight-fold coordinated and that B site occupancy is random [53]. ^{109}Ag NMR is another low-γ nucleus and an extensive study of 20 simple inorganic silver salts added a large amount of new ^{109}Ag data to the literature [54]. The suggestion has been made that given the long T_1 values encountered for ^{109}Ag 9 M aqueous $AgNO_3$ is used as the shift reference. The chemical

shift range of ^{109}Ag is large, approaching 1000 ppm for inorganic salts, with a large range of skews and spans observed. Hence the chemical shift interaction parameters are very sensitive to the local environment.

3.2 Half-integer Spin High-γ Quadrupolar Nuclei

There are a range of quadrupolar nuclei with relatively large magnetic moments (e.g. ^{45}Sc, ^{69,71}Ga, ^{63,65}Cu, ^{93}Nb, ^{113,115}In, ^{139}La) where the effective quadrupolar broadening factor (taking into account both (i) the 'raw' second-order quadrupolar broadening factor, determined by the magnetic and quadrupolar moments along with the spin, and (ii) the local electron density 'magnification' of the external EFG as estimated by the Sternheimer antishielding factor. The effective quadrupole broadening factor is then estimated by multiplying factors (i) and (ii) (defined in Table 2 of [5])) for these nuclei is in the range ~25-250 and compares to 0.6 for ^{11}B and 3.6 for ^{27}Al. Hence the significantly higher broadening requires either some of the wideline techniques or make use of the much faster spinning and higher magnetic fields available. ^{71}Ga NMR is now being increasingly used to distinguish GaO_4 and GaO_6 on the basis of their differing chemical shifts [44, 50]. The ability to distinguish and quantify these sites in materials is at approximately the same state of development as ^{27}Al was 15 years ago.

^{45}Sc static and MAS NMR spectra were reported at two applied magnetic fields from a range of simple scandium compounds including $Sc(NO_3)_3.5H_2O$ and $ScCl_3.6H_2O$. χ_Q was found to be in the range 3.9 to 13.1 MHz, with a good correlation to the local geometry of the scandium environment. Static data revealed that all the compounds had a significant CSA, with spans in the range 60 to 200 ppm, indicating that CSA should probably be taken into account in all scandium compounds [55]. A further study using MAS at three magnetic fields on a different range of model inorganic compounds found χ_Q in the range 1.6-23.4 MHz. In looking at the isotropic chemical shift range it appears that the chemical shift in these compounds was dominated by the local coordination number, with ScO_6 and ScO_8 showing a shift difference of ~200 ppm [56]. Applying ^{45}Sc MAS NMR to the solid solution $Sc_2(WO_4)_3$-$Sc_2(MoO_4)_3$ suggested a small average χ_Q of 3.6 MHz, with spectra changing in a way consistent with random mixing of the tungsten and molybdenum over tetrahedral sites [57]. Oxygen vacancy hopping is important in scandium-doped CeO_2, a solid state electrolyte. To examine the dynamics, ^{45}Sc NMR data from –80 ^{o}C up to 600 ^{o}C was collected. At low temperatures two peaks are observed at 23 and –34 ppm which are attributed to ScO_7 and ScO_8 respectively. As the temperature increases these two peaks start to coalesce as oxygen starts to exchange between sites. The oxygen vacancy hopping frequency, as

well as the activation energy, determined by NMR for this process are in agreement with values deduced from electrochemical impedance spectroscopy [58].

^{93}Nb is potentially an important probe nucleus of inorganic materials problems that could include contributing to understanding the activity, stability and selectivity of functional materials such as catalysts, catalytic supports, as well as microporous and mesoporous ion-exchangers. Solid state niobate chemistry also plays a crucial role in several very important piezoelectric phases, as well as several other technological applications such as optical materials and nuclear waste immobilisation. Although ^{93}Nb is 100% naturally abundant and has a moderately large magnetic moment there is still only a limited number of solid state NMR studies as its relatively large quadrupolar moment introduces a large second-order quadrupolar broadening. In addition, ^{93}Nb appears to exhibit a large chemical shift range (typically ~4000 ppm) with significant structural distortion producing large CSAs and significant chemical shift dispersion broadening of spectra for disordered systems. In the last decade there have been a number of studies of effectively model systems, but there is a question mark over many of the early values of the NMR interaction parameters determined because of single field analysis, imperfections in the lineshapes because of their width and the neglect of any CSA contribution to the line shapes. Hence some of the suggested shift ranges attributed to different coordinations may need to be revisited. A recent study combined data at four magnetic fields (e.g. Fig. 1b) and DFT calculations [10]. This study emphasised that a variable B_o approach unambiguously detects the presence of both quadrupolar and CSA contributions from ^{93}Nb broadline data. These data reveal that the ^{93}Nb EFG tensor is a particularly sensitive measure of the immediate and extended environments of the Nb(V) positions, with χ_Q values 0 to >80 MHz, δ_{iso} covering a range of ~250 ppm and CSA spans of 0 to ~800 ppm, with the latter being of particular note compared to several previous studies. The three method approach that uses crystal structure, NMR measurement and DFT calculation exhibits a good level of accuracy and the excellent correlations found indicated that ^{93}Nb is a good probe of local structure.

Lanthanum is another key nucleus for many important materials problems such as ferroelectric and related phases. There have been very limited solid state NMR reports of ^{139}La because of the relatively large quadrupolar interaction encountered [3]. A recent study of anhydrous lanthanum fluorides used five B_o values, as well as a combination of static and MAS approaches. Large χ_Q in the range 15.55-24.0 MHz were determined, as well as sizeable CSA, with spans up to 650 ppm. The isotropic chemical shift was observed to vary from −135 to 700 ppm and displayed an inverse halogen dependence [59].

3.3 Half-integer Spin Low-γ Quadrupolar Nuclei

The study of low-γ quadrupolar nuclei, although still limited, has seen a large increase since the area was reviewed in 2001 [51]. Nuclei in this group include ^{25}Mg, ^{33}S, ^{35,37}Cl, ^{43}Ca, ^{47,49}Ti, ^{73}Ge, ^{91}Zr, ^{95,97}Mo and ^{135,137}Ba. Examples of developments of all these nuclei can be found in the literature in the last decade, but a few illustrative cases will be given here. ^{95}Mo is potentially a very significant nucleus to probe some important catalysis problems. The $(MoO_4)^{2-}$ environment is quite symmetric. Recent studies [60, 61] have shown that in such coordinations χ_Q tends to be < ~3 MHz which makes NMR observation relatively straightforward. Static spectra reveal that there can be significant CSA interaction (Fig. 7). Multiple sites can be distinguished, with α-$ZnMoO_4$ having three crystallographically distinct molybdenum sites which are readily resolved (Fig. 7(d)), with two having clear second-order quadrupolar lineshapes and one much narrower. DFT calculations allow ready identification of the resonances with crystallographic sites on the basis of both the quadrupolar interaction and isotropic chemical shift. On moving to real catalytic materials the quadrupolar interaction in other local environments can be much larger, such that spectra have to be interpreted carefully even at high magnetic field [61]. An example of a nucleus which is now observable really for the first time because of the better availability of high magnetic field is ^{73}Ge. From the two forms of crystalline GeO_2, GeO_4 units had a much smaller χ_Q than GeO_6 and a shift difference of ~200 ppm [62].

^{33}S is another nucleus that has many potentially important inorganic materials applications, with sulphur being a component in for example cements and concretes. The quadrupolar nature, small magnetic moment and low natural abundance (0.76%) have made NMR observation of this nucleus highly problematic. Only in sites of the highest symmetry such as many S^{2-} and $(SO_4)^{2-}$ is observation straightforward. Although the shift range of sulphate is small, the shift associated with a specific charge-balancing cation appears well defined. Hence for sulphur dissolved in glasses, sulphate species could be detected, with in multiple cation glasses the shift pointing to sulphate association with specific cations [63]. The same sensitivity of the SO_4 chemical shift and χ_Q was used in some cement-related systems to distinguish the different sulphate species present, with ettringite having a very different chemical shift and lineshape from gypsum [64]. As soon as the symmetry of the local coordination drops the quadrupolar interaction rises rapidly, a point well illustrated by a series of potassium sulphates where the SO_4 units are bonded differently [65]. In isolated SO_4 χ_Q was only 0.959 MHz, but this rose rapidly to 16.2 MHz in an S_2O_7 unit. This effect was even more pronounced in sulphites where the presence of sulphur could only be detected as a very short-lived echo [63].

As with other low-γ nuclei examined here ^{25}Mg has also remained little exploited, with the odd study showing one or two spectra especially from samples with small χ_Q. This situation has very recently moved forward significantly with two studies reporting extensive sets of ^{25}Mg NMR interactions from relatively simple inorganic magnesium-containing compounds, comparing the results with DFT calculations [9, 66]. The experimental and calculated parameters show excellent correlation, generally indicating that ^{25}Mg NMR can indeed be used to probe structure. $MgSO_4 \cdot 6H_2O$ has two distinct magnesium sites, with the two contributions to the lineshape readily distinguished (Fig. 1(a)) despite the structural differences determined by XRD between them being very small. The average Mg-O bond lengths are 2.080 Å and 2.083 Å, and average O-Mg-O bond angles are 90.04° and 87.39° for sites 1 and 2 respectively, with the corresponding χ_Q of 1.65 and 2.4 MHz respectively, assigned on the basis of DFT calculations. The spectra of magnesium sulphates are very sensitive to the hydration state [9]. In diamagnetic compounds the isotropic chemical shift range is ~200 ppm, but with many shifts concentrated from –15 to 25 ppm. On the basis of the collected data so far the chemical shift could probably distinguish MgO_4 and MgO_6 in materials where magnesium's coordination was unknown.

Despite calcium making a major elemental contribution to matter on the Earth, for example being the fifth most abundant element in igneous rocks, present in most soils and sedimentary beds, the main cation in mineralised bone tissue and shells, and a component in many man-made products, such as crucially important cements, there have been very few solid state NMR studies of ^{43}Ca until the last five years. ^{43}Ca is yet another low-γ, quadrupolar nucleus with a very low natural abundance (0.14%). Despite the unpromising intrinsic NMR parameters when a natural abundance study of a wide range of calcium compounds was undertaken relatively narrow resonances were observed [67]. This meant that only modest MAS rates were necessary (4-5 kHz) so that large volume rotors could be used (typically 9.5 mm diameter). With an increasing range of observations of ^{43}Ca [68] it is clear that δ_{iso}, which is the most readily determined parameter from MAS NMR spectra, could provide information not only on the average Ca---O bond distances, but also about the nature of the next nearest neighbours around the calcium, as noted for borates and aluminosilicates [69].

A good example of the likely utility of ^{43}Ca NMR has been the study of hydroxyapatite (HA) which has two distinct calcium sites, Ca(1) which is eight-coordinated by oxygen and Ca(2) which is seven coordinate, with one of these an OH. Recording the ^{43}Ca MAS NMR spectra at three magnetic fields up to 18.8 T allowed the two sites to be separated and the individual parameters to be deduced which revealed both sites had χ_Q = 2.6 MHz, but shifts that differed by ~10 ppm. The assignment of the resonances was possible on the basis of the relative intensity of

the two sites in the structure which is 3:2 [70]. The assignment was confirmed since the Ca(2) is much closer to the proton, allowing site discrimination on the basis of the different dipolar coupling [71]. A ^{1}H-^{43}Ca REDOR experiment relies on the increased dephasing of the calcium closer to the proton. Hence the left hand side of the line (Fig. 8(a)) more strongly dephases, confirming its assignment as the Ca(2) site. More sophisticated experiments that have been developed for more abundant nuclei with larger signals can equally be applied to low-γ nuclei. As an example R^3-HMQC was applied to HA and the structurally more poorly defined oxyhydroxide t-HA [72]. The R^3-HMQC spectrum from HA shows the expected correlation between the Ca(2) site and the OH. Then in t-HA there are vacancies, which means there is a much increased range of local environments, showing up as more distinct hydroxyl environments and effectively three inequivalent calcium environments close to the hydroxyls. This means amongst the local structures are some regions that are the same as HA, but then others are associated with defects. Examining three calcium silicate glasses which contain aluminium and/or sodium showed that the ^{43}Ca NMR parameters are highly sensitive to variations in its chemical environment. In such glasses calcium changes its role from charge compensating the $(AlO_4)^-$ to acting as a network modifier being associated with non-bridging oxygens. The change of δ_{iso} and χ_Q gave clear discrimination of the different sites, allowing such changes in a series of glasses to be followed [73].

3.4 Integer spins

Although ^{11}B is a very sensitive nucleus with a relatively high frequency and can readily distinguish BO_3 and BO_4 sites and even inequivalent sites within these groups, ^{10}B offers an alternative view. It is an I = 3 nucleus and spectra have been observed using a field stepping approach and spectra built up from ‘slices’ summed together (Fig. 9(a)) to produce the broad spectra where the transitions extend over several MHz. This work used a conventional spectrometer equipped with an additional sweep coil [74, 75]. The spectra were simulated taking third-order perturbation theory into account, with an additional Gaussian broadening in glasses to reflect the distribution of environments present. The boron interaction parameters were more accurate than from ^{11}B studies. In crystalline $Cs_2O.9B_2O_3$ the structure is made up of interpenetrating networks of boroxyl rings and triborate groups (see Fig. 9(b)) in the ratio 2:1, which results in BO_3 and BO_4 environments in the ratio 8:1. The ^{10}B data clearly distinguished these sites (Fig. 9(b)). Intermediate range order in borate glasses results from the presence and connection of the multiple sites, with the quadrupolar asymmetry parameter shown to be particularly sensitive to differences in order [75]. There has also been some progress observing I =

1 nuclei such as ^{14}N with signal enhancement techniques emerging. The techniques developed are close to the WURST approach and was demonstrated for KNO_3 and was termed DEISM [76] Given the importance of nitrogen in some materials this development could allow much more frequent observation of ^{14}N as a probe of materials.

4. Exemplar Recent Applications of Solid State NMR to Inorganic Materials

Applications of solid state NMR to inorganic materials have become increasingly widespread which is a measure of the success of the technique. Many reports involved well established nuclei applied to materials that have been long studied by NMR techniques e.g. zeolites. However a very elegant use of ^{29}Si was to examine the effect of radiation damage in zircon containing α-emitters as a model nuclear waste storage medium. ^{29}Si MAS NMR of pristine zircon has a single sharp resonance from Q^0 species. The α-particle and the nuclear recoil displace atoms from their lattice sites which causes disorder. This could be readily quantified by ^{29}Si MAS NMR, and could be correlated to the radiation dose [77].

4.1 Geopolymers

^{29}Si and ^{27}Al MAS NMR of aluminosilicates was one of the early major successes of the technique in studying inorganic materials since NMR provided new insight into the local ordering which was very difficult using scattering techniques because these two elements are light and have very similar X-ray scattering factors. A relatively new area of aluminosilicate materials chemistry is that of geopolymers which are structurally disordered, but are not glasses. They are being developed as more environmentally friendly alternatives to cements. ^{1}H and ^{23}Na have also been applied and changes in compressive strength have been related to network connectivity [78]. In a range of aluminosilicate geopolymer gels detailed ^{29}Si MAS NMR studies were carried out such that the Q^4(mAl) environments could be quantified by Gaussian deconvolution. For Na-, NaK-, and K-geopolymers the Si/Al distribution showed no significant difference for materials where the Si/Al ratio was >1.65. However, for K-geopolymers at lower Si/Al ratios the concentrations of Q^4(4Al) and Q^4(3Al) were different compared to the other cation-containing geopolymers, implying the structural ordering was different with differing alkali type. Hence the potassium samples were suggested to be more disordered such that some Al-O-Al linkages are present [79]. ^{29}Si NMR is a good probe of the changing nature of the geopolymer network even in the presence of zeolites and metakaolin because their spectral parameters are well known and can be readily separated from the resonances of the network. Increased connectivity as deduced from the ^{29}Si could be directly correlated to the compressive strength [80]. There was interesting contrast between the ^{29}Si and ^{27}Al NMR data with the latter showing less disorder around the AlO_4 sites

within the structure. ^{23}Na data interestingly suggests that although there are several different environments none of these are directly attributable to terminating the geopolymer network which could be a cause of structural weakening.

To further illustrate the importance of a multinuclear approach, to include even less studied nuclei when possible, a series of aluminosilicate geopolymers have been examined containing up to 50 wt% of added calcium compounds [81]. The level of calcium added was high to allow natural abundance ^{43}Ca MAS NMR spectra to be acquired. The change of the ^{43}Ca MAS NMR spectrum from that of the initial compound as the reaction proceeds suggest that the calcium enters the network when the calcium starts as a calium silicate phase (e.g. gel) or $Ca(OH)_2$. However geopolymers initially containing $CaCO_3$ and $Ca_3(PO_4)_2$ show ^{43}Ca MAS NMR spectra that are virtually unchanged from those of the initial calcium compound. In this case the implication is that the calcium phase is acting as a filler and does not enter the geopolymer network.

4.2 Biomaterials

Biomaterials science has undoubtedly become much more important in the last decade with very many more research programmes looking at tissue replacement and implanted drug release systems. Such materials can be complex multiphase, poorly ordered mixtures. For example to provide materials with significant strength, flexibility and ability to stimulate cell growth can be very demanding. Often these can be only delivered by hybrid materials and the local structure and the bonding between the components can be important. Bioglasses are a very important class of biomaterials and sol-gel processed samples often show better cellular response than a similar glass formed by conventional melt-quench techniques. One of the factors that imparts the superior properties is the higher surface proton content of the sol-gel produced glass. Proton quantification via ^{1}H NMR on weighed samples is a very straightforward method to determine the proton content of sol-gel produced materials [82].

NMR spectroscopy of biomaterials has significantly developed such that now as well as simple 1D MAS, complex pulse sequences to identify different structural species present are used in combination with calculations of the expected NMR parameters to help with interpretation. A range of proton-containing phosphate materials, important in biomaterials developments, including $CaHPO_4.2H_2O$ were examined by 33 kHz MAS at 17.6 T giving partial resolution of five signals with the acid POH significantly shifted from the other protons at 10.2 ppm. However the make-up of the rest of the spectrum from different components could only be unambiguously simulated by basing the relative shift positions on the values obtained from first principles calculations. In another related phase β-$Ca(PO_3)_2$ there are corner-sharing PO_4 chains and first

principles calculations can help in the assignment of the peaks, but this is not possible for the PO_4 units designated P1 and P3 and a 2D MAS-J-INADEQUATE sequence was necessary to elucidate the connectivity and hence the identity of the sites (Fig. 10) [83]. In octacalcium phosphate the phosphorus sites were assigned from ^{31}P DQ and ^{31}P-^{1}H HETCOR measurements and it was shown that a substantial fraction of the phosphate groups had been converted to hydrogen phosphates [84]. Another example of the use of a combined methodology was a study on some mesoporous CaO-SiO_2-P_2O_5 glasses that combined 1D ^{1}H, ^{29}Si and ^{31}P MAS NMR with CP, DQ ^{1}H-^{1}H experiments and heteronuclear correlation experiments. The combination allowed the spatial distribution of the different elements to be understood and a biphasic model of the structure to be proposed [85]. The pore wall is mainly SiO_2 with a nanoscale amorphous calcium orthophosphate phase that is distributed heterogeneously on the inner surface. This distribution of elements means that the calcium and phosphorus are readily exchangeable with fluids in contact with the surface.

The ‘classic’ natural biomaterials are bone and related materials such as tooth enamel and dentin, which are effectively composite materials consisting of an organic matrix (primarily collagen type I) deposited on nanocrystals of a mineral inorganic phase commonly based on hydroxyapatite (HA). Nanocrystalline HA was shown by ^{1}H and ^{31}P NMR to correspond to calcium-deficient HA as a core with a surface layer dominated by hydrogen phosphate groups and structural water [86]. The structural complexity HA is that it can accommodate a whole range of ionic substitutions such as CO_3^{2-}, F^-, Na^+ and Mg^{2+}. CO_3^{2-} is a very important substitution and although substitution levels of other ions can be very low they can have a strong influence on the functional properties. Although solid state NMR is an obvious probe of the atomic scale substitutions in apatite-based natural materials and although some studies were performed some time ago it is only recently that NMR has emerged as a key analytical tool for these materials [87]. Borate substitution with the HA structure formed at high temperature shows that the bulk of the borate units are incorporated in a disordered calcium phosphate phase as a surface layer that [88]. The interface between the HA core and the amorphous phosphate surface layer was probed by a combination of triple resonance ^{1}H-^{31}P-^{11}B CP and ^{31}P{^{1}H} REDOR [88]. In mineralised cartilage the inorganic surface species that interact with the organic surroundings have been probed by 1D ^{1}H and ^{31}P, 2D ^{13}C{^{31}P} heteronuclear correlation and ^{13}C{^{31}P} REDOR experiments [89]. The surface structure was shown to be very similar to that in bone and the organic species interacting were readily identified [89]. An NMR study that combined 1D and 2D techniques such as ^{1}H-^{31}P HETCOR examined subchondral regions of equine joints where there was evidence of osteoarthritic disease. The results did not find any differences in the structures as revealed by

NMR between diseased and healthy inorganic components which suggest that the disease may be more related to the organic component matrix or its interaction with the mineral [90].

In formation of biological HA, octacalcium phosphate (OCP) is a supposed precursor phase. NMR, as a component technique, has probed the molecular mechanism of the transformation of OCP to HA, where ^{31}P DQ has proved to be particularly informative with eight sets of auto- and cross-correlation peaks assigned to the OCP phase [91, 92]. The DQ signals can be monitored as a function of mixing time and the time variation can be modelled. The key point is that the modelled variation can be compared to the expected variation in the phosphorus separations as the structure transforms to HA, with the data suggesting that OCP crystals transform to HAp topotaxially. Water interaction is also important and CP suggests that water enters the hydration layers of an hydrolysis reaction [92]. Natural abundance ^{43}Ca MAS NMR of a cow tooth and horse bone revealed broader spectral lines than from synthetic HA, with chemical shift dispersion dominating the linewidths revealing greater atomic disorder. Sodium substitution examined via ^{23}Na MAS NMR at different magnetic fields, in combination with 3Q-MAS, ^{23}Na{^{31}P} REDOR and ^{1}H{^{23}Na} R^{3}-HMQC clearly showed that sodium is located inside the apatite phase [93]. ^{31}P NMR has been used to examine rat dentins of various ages and a picture is presented of apatite crystallites embedded in an amorphous matrix, with ~19% of the apatite crystallites containing hydroxyls [94].

4.3 Paramagnetic Systems

The presence of paramagnetic species is often regarded as detrimental to obtaining high resolution NMR spectra because of the broadening effects that such ions can introduce. However there have long been studies that have explored the shift dependence on the geometrical situation of the different sites relative to the paramagnetic species, thereby allowing comment on the siting of the species. This has been used for some time in inorganic systems where at low concentrations the shifts can be detected and the broadening effects are not too severe. A good practical example is in the substitution of Rare Earth (RE) ions in materials used as phosphors where the distribution of the RE (i.e. homogeneous or clustered) can have profound effects on the properties (Ref. 3 reviews this up to 2001). A more recent example is transition metal ion doping of zircon which is an industrially important pigment. The colour depends on the nature of the dopant and its distribution. V^{4+} is a common addition in such zircon pigments and normal ^{29}Si MAS NMR was able to show the dominant unaffected resonance and then three smaller, shifted resonances were clearly observed that could be assigned to V^{4+} sitting on the zirconium, silicon and in interstitial sites. The assignment of the sites was possible on the basis of the relative shifts of the different

sites from the expected hyperfine fields [95]. The site preferences and how these varied with concentration could be readily followed.

The availability of increasingly fast MAS has seen an increase in the number of studies of paramagnetic materials. For example in pyrope $[Mg,Fe]_3Al_2Si_3O_{12}$ for ^{27}Al and ^{29}Si a pseudocontact interaction was observed as Fe^{2+} was added. The effects observed were an increase in sideband intensities and new peaks as Fe^{2+} substituted as a second nearest neighbours. The study pointed out that some peaks, those too close to the iron, are lost from the spectrum and hence careful absolute intensity comparisons are sometimes necessary [96]. Energy-related materials such as lithium batteries are now intensively investigated. In rechargeable batteries $LiCoO_2$ is an important cathode material, but there has been an attempt to reduce the cobalt content because of the cost of cobalt has seen its replacement to varying extents by nickel and manganese which broaden the lithium lines in such materials. Although ^6Li has a much smaller magnetic moment than ^7Li its much smaller quadrupolar moment means that different sites can be more readily distinguished and cation motion can be examined via changes in the spectra with temperature. 30 kHz MAS at 4.7 T [97] showed three different local lithium environments in $Li[Ni_{0.33}Mn_{0.33}Co_{0.33}]O_2$ which were attributed to different Ni/Mn/Co next nearest neighbour environments. Other really interesting lithium-based cathode materials are $LiFePO_4$ [98] and $Li_3V_2(PO_4)_3$ [99]. In these materials the advantage of really fast MAS is well demonstrated. At low MAS the resonances only partially break up, such that only at 40 kHz do the three ^{31}P centrebands stand out from the spinning sidebands [99] (Fig. 11). The resonances shifted to such high frequency result from the hyperfine transfer of electron density from the V^{3+} and can be assigned on the basis of the anticipated different Fermi contact interactions.

4.4 Energy Materials – Lithium Ion Batteries, Fuel Cells and Hydrogen Storage

Fuel cells and battery related materials are technologically very important and the ability to develop new materials and understand the structural relation of the key properties means that NMR is an important physical probe that has found increasing use over the last decade. Organic materials play a central role in many energy materials technologies, but again this review specifically concentrates on NMR as a probe of inorganic materials. There are several specific, complementary technologies where NMR has already made important contributions such as hydrogen storage materials, lithium ion batteries and oxygen ion conductors. Hydrogen storage materials with the necessary combination of storage capacity and temperature/pressure of operation are crucially important for the maximum potential impact of the hydrogen economy. The location and motion of hydrogen within such materials is of paramount importance such that

an atomic scale probe, such as NMR can play a central role in understanding and optimising such materials. These materials can often be complex, nanocrystalline phase mixtures containing metallic and insulating components which means that wide shift ranges should be investigated. $NaAlH_4$ is a potential hydrogen storage material and ^{27}Al NMR revealed that there was an surface alumina layer, with various proton sites revealed by ^{1}H MAS NMR [100]. In $NaAlH_4$ nanocomposites with carbon the confinement in nanopores causes the ^{23}Na and ^{27}Al spectra to be broadened from increased disorder. As dehydrogenation is followed a single release peak was observed and at maximum dehydrogenation a peak from metallic sodium occurs. Rehydrogenation restored the solid state NMR spectra indicating that process is reversible for a $NaAlH_4$/C composite [101].

Much of our mobile technology depends on the availability of suitable power sources and lithium ion batteries play a crucial role in this. Detailed understanding of the role played by the electrolyte and the electrode materials in such systems is necessary. Layered lithium compounds such as Li_xMO_2 materials play the central role as the positive electrode, with replacements for simple compounds, such as the widely used $LiCoO_2$, being sought because of higher lithium capacity. Many of the contenders are more complex solid solutions, with transition metal ion layers which can accommodate additional lithium. Fast MAS (up to 38 kHz) on a lithium nickel manganese compound revealed several peaks corresponding to differing numbers of Mn/Ni neighbours [102]. Extending this to a more complex compound also containing significant cobalt content the ^{6}Li MAS NMR was dominated by all cobalt in both the first and second neighbour shells. The distribution of Mn/Ni in these shells could be followed by a range of additional peaks spread over > 500 ppm and the changes with lithium content were readily followed [103]. ^{6}Li has been used to detect the different lithium sites, separated by differing disposition relative to the paramagnetic centre. 2D exchange spectra revealed the activation energy of lithium hopping between different sites and has been applied to novel potential electrode materials such as $Li_5V(PO_4)F_2$ [104] and $Li_3Fe_2(PO_4)_3$ [105]. One of the most elegant studies on lithium-related battery problems was to combine ^{7}Li MAS and *in situ* static work. The observation was made that *ex situ* studies were sensitive to the time taken to dismantle the cell, such that *in situ* work is crucial to get a real understanding. An *in situ* NMR cell was presented to look at the intercalation of lithium into silicon, which is the negative electrode in such batteries, with observations made on an actual working battery. Lithium insertion into silicon occurs creating a crystalline-to-amorphous transition. A range of lithium coordinations could be observed with the changes with charge/discharge followed [106].

Materials used as electrolytes in fuel cell applications have been widely studied and oxygen ion conductors are important in this role. Apatite-structured oxygen ion conductors have generated much interest in this role with materials based around $La_{9.33}(SiO_4)_6O_2$ which has cation vacancies and $La_{9.67}(SiO_4)O_{2.5}$ which has oxygen excess sites in addition to the vacancies. The conductivity was very much better in the oxygen excess sample. ^{29}Si NMR was able to detect the oxygen excess with the appearance of a second peak in the MAS NMR spectrum attributed to Q^0 species adjacent to an interstitial oxygen. At other compositions peaks associated with condensation to form Q^1 species can also be seen [107]. Oxygen motion itself needs to be understood and in a material such as ZrW_2O_8 a ratcheting mechanism between the WO_4 units explained the variable temperature ^{17}O data [108]. ^{17}O NMR data was collected over an extended temperature range (–238 to 1000 ^{o}C) on the anionic conductor $Bi_{26}Mo_{10}O_{69}$. This material contains isolated $(MoO_4)^{2-}$and bismuth oxygen columns with two clear ^{17}O resonances observed attributable to these two species at low temperature which employed a cryoMAS probe. Variable temperature analysis showed that at lower temperatures the molybdate units were in rapid rotation whereas the bismuth-related sites were static. At higher temperatures all oxygen sites become involved in the oxygen motion [109]. The higher temperature mechanism is such that it allows long-range oxygen conduction without the need for multiple coordinated breaking of Mo-O bonds. Hence the ability of NMR to probe local structure and dynamics can be important to understand such materials.

4.5 Connectivity and Ordering in Glasses

The development of more advanced sequences, especially those which produce information about the connectivity from correlation experiments have been increasingly applied to glassy inorganic materials. For phosphate glasses, the NMR chemical shifts in 1D spectra can distinguish the differently connected P_n species (e.g. Fig. 12), with n indicating the number of bridging oxygens. The connectivity of the P_n groups can be revealed by 2D spectra, which probe the through-space dipolar or through-bond J-coupling between P_n groups via a range of correlation experiments. In the ^{31}P 2D refocused INADEQUATE spectra such as in Figure 12(c) P_1–P_1, P_1–P_2, P_2–P_1 and P_2–P_2 2D DQ peaks are observed due to the connectivities of phosphate tetrahedra present in the glass. A modified sequence was suggested by appending a spin-echo, termed the INADEQUATE spin-Echo (REINE) experiment. The J-couplings, although often not resolvable can be quantitatively determined by a spin-echo refocusing the effect under chemical shift offsets as found in disordered samples. The REINE experiment applied to a CdO-P_2O_5 glass reveals 2D distributions of both ^{2}JP;P couplings and spin-echo dephasing times (T_{02}) which are correlated

with changes in the ^{31}P SQ and DQ chemical shifts. These variations in ^{2}JP;P constitute a potentially rich new source of information for the characterisation of variations in bond angle and bond length. The REINE experiment unambiguously reveals differences in the J-couplings between a P_1 and a P_2 unit ($^{2}JP_1;P_2$) and those between two P_1 units ($^{2}JP_1;P_1$) or two P_2 units ($^{2}JP_2;P_2$). These spectra have been shown to be sensitive to the PO_4 chain lengths. The observed spectral features, especially the distributions of parameters can be compared to first principle calculations of J-couplings [110].

In the phosphate glasses $(NaPO_3)_{1-x}(B_2O_3)$ $(0 \leq x \leq 0.3)$ a combination of NMR sequences was used to examine changes in linkages as the composition was varied. From 1D spectra it looks as though BO_4 units are connected to P_2 and P_3 units. At compositions with $x \leq 0.2$ all the boron is present as $(BO_4)^-$ and hence the charge balance means that the non-bridging bonds on the phosphate network decrease and the connectivity of the network increases, reflected directly in the increase in the glass transition temperature. The REDOR curves modelled on the basis of the dipolar coupling allows the spatial distribution of the atoms to be examined, and suggest P-O-B linkages tend to cluster with the P_3 unit attracting two BO_4 neighbours [111]. For aluminophosphate glasses the 100% natural abundance of both ^{27}Al and ^{31}P allowed a combination of 1D MAS, MQMAS and ^{31}P-{^{27}Al} HETCOR to provide detailed speciation information. The interconnection to the aluminophosphate groups to form the network was elucidated via ^{31}P{^{27}Al} HMQC, REAPDOR and HETCOR, as well as ^{27}Al{^{31}P} REDOR. The P-O-P connectivity was probed by 2D J-resolved experiments. The whole range of P_n units was present and their connectivity to AlO_x (x = 4, 5, 6) species were identified and quantified so that a real model of the intermediate order could be advanced [112]. In mixed cation alkali borate glasses again a combination of NMR methods including ^{11}B{^{23}Na} REDOR and the alkali-alkali interactions elucidated via SEDOR experiments showed that cations were randomly mixed in the structure. These observations help explain the mixed alkali effect as a site mismatch phenomenon [113].

J-couplings have also been studied in highly ^{29}Si-enriched calcium silicates. The very small linewidths in crystalline $CaSiO_3$ (wollastonite) polymorphs allowed ^{2}J couplings as low as 1.5 Hz to be accurately determined, as well as allowing the first observation of strong J-coupling in such spectra spectra from an inorganic solid. A relationship was deduced between the ^{2}J coupling and the Si-O-Si bond angle which then for the glass allowed the bond angle distribution to be determined for each of the Q^n species [114]. In aluminosilicate glasses the ability to distinguish and fit ^{29}Si MAS NMR spectra where several different, but poorly resolved Q^4(mAl) species are present is extremely important to constrain the Si,Al distribution. Sequences that can use the coupling, such as 4Q filtered INADEQUATE can pick up the number of differing

neighbours (in a 100% ^{29}Si labelled system) by sequentially increasing the mixing time and this information can be used to constrain the fits of the 1D spectrum [115]. {^{17}O}^{27}Al HMQC experiments readily separate the Ca-O-Al and (Si,Al)-O-(Si,Al) linkages. In a magnesium aluminoborate glass the ^{27}Al DQ MAS NMR data clearly showed that there was preferential proximity between the AlO_4 and AlO_5, with no connection to the AlO_6 present, suggesting that the AlO_6 are connected together in separated clusters (Fig. 12(e)) [116].

With *ab initio* calculations playing an increasing role in providing more detailed structural interpretation of the NMR interaction parameters, extension to amorphous materials is being developed. The DFT methods rely on the spatial periodicity of the structure. This is mimicked in disordered material by taking a supercell. This approach was applied to a sodium silicate tetrasilicate glass with the parameters compared to some closely related crystalline sodium silicate phases. The glassy structure generated from molecular parameters provided the basis of the sueprcell to calculate the NMR parameters and gave really good agreement to the experimentally determined values. The relationships deduced between the NMR parameters and structure increases the certainty of the implications for structure of the distributions of NMR parameters determined [117]. To illustrate this, a very detailed analysis was carried out on the archetypal inorganic glass, vitreous silica. GIPAW calculations were combined with hybrid Monte Carlo/molecular dynamics simulations to understand the connection between the various ^{17}O and ^{29}Si NMR parameters and their distribution to the local structure in terms of Si-O bond lengths and Si-O-Si bond angles. This allowed a new analytical model to be proposed for the reconstruction of the Si-O-Si bond angle. This looks highly promising given its ability to reproduce both the mean bond angle and its distribution using the ^{17}O and ^{29}Si experimental data on the same samples [118]. Comparison of calculated parameters to experimental values in disordered materials offers exciting new opportunities for better understanding of the structure of disordered materials.

5. Summary and Outlook

Even though high resolution solid state NMR has been applied to inorganic materials for more than 30 years the capability of the technique still continues to increase very rapidly. For example, rather than just a few common nuclei (e.g. ^{23}Na, ^{27}Al, ^{29}Si, ^{31}P) an increasingly multinuclear approach is now possible opening up some exciting possibilities and this will only continue. Some of the main developments within the last decade have been:

1. The availability of much higher magnetic fields (e.g. >17.6 T) for solid state NMR and ultrafast MAS (e.g. beyond 45 kHz).

2. The availability of high resolution techniques for half-integer quadrupolar nuclei such as MQMAS, STMAS and DOR.
3. Increased observation of nuclei with small magnetic moments encouraged by 1 above, and by signal enhancement via manipulation of satellite transition populations.
4. The increasing translation and development of correlation sequences to solids providing connectivity information and hence new insight into medium-range order in materials, including those showing disorder.
5. The role of first principles calculations of the NMR interactions which are closely integrated with their experimental determination giving new structural insight.

The enhanced NMR capability can be applied to many areas of materials science and technology. Examples that are exciting a lot of interest currently such as biomaterials and geopolymers are likely to be the subjects of many more solid state NMR studies.

Acknowledgements

The NMR infrastructure at Warwick is funded through a variety of sources including EPSRC, the HEFCE and the University of Warwick, as well as through the Science City Advanced Materials project supported by Advantage West Midlands (AWM) and part funded by the European Regional Development Fund (ERDF) for which the authors are grateful. Copyright holders who gave permission for the use of figures from their publications are thanked.

Summary of NMR abbreviations used

1D – One dimensional
2D – Two dimensional
CASTEP – Cambridge serial total energy package
CP – Cross polarisation
CSA – Chemical shift anisotropy
CT – Central transition
DEISM – Direct enhancement of integer spin magnetisation
DFS – Double frequency sweeps
DFT – Density functional theory
DOR – Double angle rotation
DQ – Double quantum
DQF – Double quantum filter
EFG – Electric field gradient
GIPAW – gauge-including projector augmented wave
HETCOR – Heteronuclear correlation
HMQC – Heteronuclear multiple quantum correlation
HSQC – Heteronuclear single quantum correlation
HS – Hyperbolic secant
INADEQUATE – Incredible natural abundance double quantum transfer experiment

INEPT – Insensitive nuclear enhancement by polarisation
MAS – Magic angle spinning
MQ – Multiple quantum
PT – Polarisation transfer
QCPMG – Quadrupole Carr Purcell Meiboom Gill
RAPT – Rotor assisted population transfer
REAPDOR – Rotational echo adiabatic passage double resonance
REDOR – Rotational echo double resonance
REINE – Refocused INADEQUATE spin-echo
SEDOR – Spin-echo double resonance
S/N – Signal to noise
ST – Satellite transition
STARTMAS – Satellite transitions acquired in real time MAS
WURST – Wideband uniform rate and smooth truncation
VOCS – Variable offset cumulative spectroscopy

References

[1] E. Lippmaa, M. Magi, A. Samoson, G. Engelhardt, A.R. Grimmer, J. Am. Chem. Soc. 102 (1980) 4889.
[2] G. Engelhardt, D. Michel, High Resolution Solid State NMR of Silicates and Zeolites, 1987, Wiley, Chichester.
[3] K.J.D. MacKenzie, M.E. Smith, Multinuclear Solid State NMR of Inorganic Materials, 2002, Pergamon Press, Oxford
[4] A. Medek, J.S. Harwood, L. Frydman, J. Am. Chem. Soc., 117 (1995) 12779.
[5] E.R.H. van Eck, M.E. Smith, Prog. Nucl. Magn. Reson. Spectrosc. 34 (1999) 159.
[6] S.E. Ashbrook, Phys. Chem. Chem. Phys. 11 (2009) 6892.
[7] S.E. Ashbrook, M.E. Smith, Chem. Soc. Rev. 35 (2006) 718.
A review of ^{17}O NMR that provides background to the NMR interactions and techniques that are relevant to its study in the solid state and a range of applications examined.
[8] S.C. Kohn, M.E. Smith, P.J. Dirken, E.R.H. Van Eck, A.P.M. Kentgens, R. Dupree, Geochim. Cosmochim. Acta 62 (1998) 79.
[9] L.S. Cahill, J.V. Hanna, A. Wong, J.C.C. Freitas, J.R. Yates, R.K. Harris, M.E. Smith, Chem. Eur. J. 15 (2009) 9785.
[10] J.V. Hanna, K.J. Pike, T. Charpentier, T.F. Kemp, M.E. Smith, B.E.G. Lucier, R.W. Schurko, L.S. Cahill, Chem. Eur. J. 16 (2010) 3222.
An extensive state of the art NMR study of ^{93}Nb in the solid state that combines static and MAS measurements at multiple magnetic fields with DFT calculations. This work questions the accuracy of some of the parameters determined previously in the literature.
[11] A. Samoson, T. Tuherm, J. Past, A. Reinhold, T. Anupold, I. Heinmaa, Topics in Current Chemistry 246 (2005) 15.
[12] A.P.M. Kentgens, J. Bart, P.J.M. van Bentum, A. Brinkman, E.R.H. van Eck, J.G.E. Gardeniers, J.W.G. Janssen, P. Knijn, S. Vasa, M.H.W. Verkuijlen, J. Chem. Phys. 128 (2008) 052202.
The theoretical background and practical implementation of microcoil design are examined.
[13] K. Yamauchi, J.W.G. Janssen, A.P.M. Kentgens, J. Magn. Reson. 167 (2004) 87.
[14] D. Sakellariou, G. Le Goff, J.F. Jacquinot, Nature 447 (2007) 694.
[15] A. Samoson, E. Lippmaa, A. Pines, Molec. Phys. 65 (1988) 1013.
[16] I. Hung, A. Wong, A.P. Howes, T. Anupold, J. Past, A. Samoson, X. Mo, G. Wu, M.E. Smith, S.P. Brown, R. Dupree, J. Magn. Reson. 188 (2007) 246.

[17] A.P.M. Kentgens, E.R.H. van Eck, T.G. Aiithkumar, T. Anupold, J. Past, A. Reinhold, A. Samoson, J. Magn. Reson. 178 (2006) 221.
[18] I. Hung, A. Wong, A.P. Howes, T. Anupold, J. Past, A. Samoson, M.E. Smith, D. Holland, S.P. Brown, R. Dupree, J. Magn. Reson. 197 (2009) 229.
[19] J. Kanellopoulos, D. Freude, A. Kentgens, Solid State Nucl. Magn. Reson. 32 (2007) 99.
[20] Z.H. Gan, J. Am. Chem. Soc. 122 (2000) 3242.
[21] S.E. Ashbrook, S. Wimperis, J. Magn. Reson. 156 (2002) 269.
[22] S.E. Ashbrook, S. Wimperis, Prog. Nucl. Magn. Reson. Spectrosc. 45 (2004) 53.
The definitive review of STMAS, extensively developing the theoretical background along with the practical implementation and illustrated via a series of examples.
[23] S.E. Ashbrook, A.J. Berry, W.O. Hibberson, S. Steuernagel, S. Wimperis, Amer. Mineral. 90 (2005) 1861.
[24] M.J. Thrippleton, T.J. Ball, S. Steuernagel, S. Steuernagel, S.E. Ashbrook, S. Wimperis, Chem. Phys. Lett., 431 (2006) 390.
[25] R. Bhattacharya, L. Frydman, J. Am. Chem. Soc., 128 (2006) 16014.
[26] D. Massiot, I. Farnan, N. Gautier, D. Trumeau, A. Trokiner, J.P. Coutures, Solid State Nucl. Magn. Reson. 4 (1995) 241.
[27] R. Siegel, T.T. Nakashima, R.E. Wasylishen, Concepts Magn. Reson. 26A (2005) 47.
[28] R. Siegel, T.T. Nakashima, R.E. Wasylishen, Concepts Magn. Reson. 26A (2005) 61.
[29] Z. Yao, K.T. Kwak, D. Sakellariou, L. Emsley, P.J. Grandinetti, Chem. Phys. Lett. 327 (2000) 85.
The first instance of the RAPT concept being applied to non-integer spin quadrupolar nuclei to provide signal enhancement an approach that is now widely used with a number of variants.
[30] J. Haase, M.S. Conradi, Chem. Phys. Lett. 209 (1993) 287.
[31] E. Kupce, R. Freeman, J. Magn. Reson. 115 (1995) 273.
[32] D. Iuga, A.P.M. Kentgens, J. Magn. Reson. 158 (2002) 65.
[33] L.A. O'Dell, K. Klimm, J.C.C. Freitas, S.C. Kohn, M.E. Smith, Appl. Magn. Reson. 35 (2008) 247.
[34] M. Feike, R. Graf, I. Schnell, C. Jager, H.W. Spiess, J. Am. Chem. Soc. 118 (1996) 9631.
[35] L.A. O'Dell, P. Guerry, A. Wong, E.A. Abou Neel, T.N. Pham, J.C. Knowles, S.P. Brown, M.E. Smith, Chem. Phys. Lett. 455 (2008) 178.
[36] D. Iuga, C. Morais, Z.H. Gan, D.R. Neuville, L. Cormier, D. Massiot, J. Am. Chem. Soc. 127 (2008) 11540.
[37] M. Edén, Solid State Nucl. Magn. Reson. 36 (2009) 1.
[38] J.P. Amoureux, J. Trébosc, L. Delevoye, O. Lafon, B. Hu, Q. Wang, Solid State Nucl. Magn. Reson. 35 (2009) 12.
[39] A.Y.H. Lo, M. Edén, Phys. Chem. Chem. Phys. 10 (2008) 6635.
[40] T.F. Kemp, M.E. Smith, Solid State Nucl. Magn. Reson. 35 (2009) 243.
[41] D. Massiot, F. Fayon, M. Capron, I. King, S. LeCalve, B. Alonso, J.-O. Durand, B. Bujoli, Z. Gan, G. Hoatson, Magn. Reson. Chem. 40 (2002) 70.
The paper that introduces the Dmfit program that is widely used to simulate and fit NMR spectra from solids.
[42] M. Bak, T. Rasmussen, N.C. Nielsen, J. Magn. Reson. 147 (2000) 296.
[43] K. Eichele, R.E. Wasylishen, WSolids NMR Simulation Package URL http://ramsey.chem.ualberta.ca/software/software.html
[44] L.A. O'Dell, S.L.P. Savin, A.V. Chadwick, M.E. Smith, Appl. Magn. Reson. 32 (2007) 527.
[45] J.B.D. Lecaillerie, C. Fretigny, D. Massiot. J. Magn. Reson. 192 (2008) 244.
[46] G. Le Caer, B. Bureau, D. Massiot, J. Phys. Condens. Matter 22 (2010) 065402.
[47] K. Schwarz, P. Blaha, G.K.H. Madsen, Comp. Phys. Comm. 147 (2002) 71.

[48] M.D. Segall, P.J.D. Lindan, M.J. Probert, C.J. Pickard, P.J. Hasnip, S.J. Clark, M.C. Payne, J. Phys. Condens. Matter, 14 (2002) 2717.
[49] C.J. Pickard, F. Mauri, Phys. Rev. B 63 (2001) 245101.
[50] D.S. Middlemiss, F. Blanc, C.J. Pickard, C.P. Grey, J. Magn. Reson. 204 (2010) 1.
[51] M.E. Smith, Ann. Rep. Nucl. Magn. Reson. Spectrosc. 43 (2001) 121.
[52] S.E. Ashbrook, K.R. Whittle, G.R. Lumpkin, I. Farnan, J. Phys. Chem. B 110 (2006) 10358.
[53] S.W. Reader, M.R. Mitchell, K.E. Johnston, C.J. Pickard, K.R. Whittle, S.E. Ashbrook, J. Phys. Chem. C 113 (2009) 18874.
[54] G.H. Penner, W. Li, Inorg. Chem. 43 (2004) 5588.
[55] A.J. Rossini, R.W. Schurko, J. Am. Chem. Soc. 128 (2006) 12638.
[56] N. Kim, C.H. Hsieh, J.F. Stebbins, Chem. Mater. 18 (2006) 3855.
[57] N. Kim, J.F. Stebbins, Chem. Mater. 21 (2009) 309.
[58] H.J. Avila-Paredes, P.Jain, S. Sen, S. Kim, Chem. Mater. 22 (2010) 893.
[59] K.J. Ooms, K.W. Feindel, M.J. Willans, R.E. Wasylishen, J.V. Hanna, K.J. Pike, M.E. Smith, Solid State Nucl. Magn. Reson. 28 (2005) 125.
[60] A.M. Forgeron, R.E. Wasylishen, Phys. Chem. Chem. Phys. 10 (2008) 574.
[61] J.B.D. Lecaillerie, Z. Gan, Appl. Magn. Reson. 32 (2007) 499.
[62] V.K. Michaelis, P.M. Aguiar, V.V. Terskikh, S. Kroeker, Chem. Comm. 2009 4660.
[63] S. Couch, A.P. Howes, S.C. Kohn, M.E. Smith, Solid State Nucl. Magn. Reson. 26 (2009) 203.
[64] J.B.D. Lecaillerie, F. Barberon, B. Besson, P. Fonollosa, H. Zanni, V.E. Fedorov, N.G. Naumov, Z. Gan, Cem. Concr. Res. 36 (2006) 1781.
[65] I. Moudrakovskii, S. Lang, J. Ripmeester, J. Phys. Chem. A 114 (2010) 309.
[66] P.J. Pallister, I.L. Moudrakovski, J.A. Ripmeester, Phys. Chem. Chem. Phys. 11 (2009) 11487.
[67] Z. Lin, M.E. Smith, F.E. Sowrey, R.J. Newport, Phys. Rev. B 69 (2004) 224107.
[68] D.L. Bryce, E.B. Bultz, D. Aebi, J. Am. Chem. Soc. 130 (2008) 9282.
[69] C. Gervais, D. Laurencin, A. Wong, F. Pourpoint, J. Labram, B. Woodward, A.P. Howes, K.J. Pike, R. Dupree, F. Mauri, C. Bonhomme, M.E. Smith, Chem. Phys. Lett. 464 (2008) 42.
An example of the application of ^{43}Ca MAS NMR applied to phosphates, with issues concerning chemical shift referencing for ^{43}Ca discussed in detail.
[70] D. Laurencin, A. Wong, R. Dupree, M.E. Smith, Magn. Reson. Chem. 46 (2008) 347.
[71] D. Laurencin, A. Wong, J.V. Hanna, R. Dupree, M.E. Smith, J. Am. Chem. Soc. 130 (2008) 2412.
[72] A. Wong, D. Laurencin, R. Dupree, M.E. Smith, Solid State Nucl. Magn. Reson. 35 (2009) 32.
[73] F. Angeli, M. Gaillard, P. Jollivet, T. Charpentier, Chem. Phys. Lett. 440 (2007) 324.
[74] D. Holland, S.A. Feller, T.F. Kemp, M.E. Smith, A.P. Howes, D. Winslow, M. Kodama, Phys. Chem. Glasses 48 (2007) 1.
[75] J. Berkowitz, M.R. McConnell, K. Tholen, S. Feller, M. Affaigato, S.W. Martin, D. Holland, M.E. Smith, T.F. Kemp, Phys. Chem. Glasses 50 (2009) 372.
[76] L.A. O'Dell, R.W. Schurko, J. Am. Chem. Soc. 131 (2009) 6658.
[77] I. Farnan, H. Cho, W.J. Weber, Nature 445 (2007) 190.
[78] P. Duxson, J.L. Provis, G.C. Lukey, S.W. Mallicoat, W.M. Kriven, J.S.J. van Deventer, Coll. Surf. A. 269 (2005) 47.
[79] P. Duxson, J.L. Provis, G.C. Lukey, F. Separovic, J.S.J. van Deventer, Langmuir, 21 (2005) 3028.
^{29}Si NMR is shown to be a sensitive probe of the Si,Al ordering within geopolymers and that differing cations can affect this ordering.
[80] M.R. Rowles, J.V. Hanna, K.J. Pike, M.E. Smith, B.H. O'Connor, Appl. Magn. Reson. 32 (2007) 663.

[81] K.J.D. MacKenzie, N. Rahner, M.E. Smith, A. Wong, J. Mater. Sci. 45 (2010) 999.
[82] S. Lin, C. Ionescu, K.J. Pike, M.E. Smith, J.R. Jones, J. Mater. Chem. 25 (2009) 1276.
[83] F. Pourpoint, C. Gervais, I. Bonhomme-Coury, T. Azaïs, C. Coelho, F. Mauri, B. Alonso, F. Babonneau, C. Bonhomme, Appl. Magn. Reson. 32 (2007) 435.

A nice example of combining fast ^{1}H MAS, ^{31}P DQ and first principles calculations to provide a detailed assignment of some phosphates important in biomaterials chemistry.

[84] Y.H. Tseng, J.H. Zhan, K.S.K. Lin, C.Y. Mou, J.C.C. Chan, Solid State Nucl. Magn. Reson. 26 (2004) 99.
[85] E. Leonova, I. Izquierado-Barba, D. Arcos, A. López-Noriega, H. Hedin, M. Vallet-Regi, M. Edén, J. Phys. Chem. C 112 (2008) 5552.
[86] C. Jager, T. Welzel, W. Meyer-Zaika, M. Epple, Magn. Reson. Chem. 44 (2006) 573.
[87] W. Kolodziejski, Topics Curr. Chem. 246 (2005) 235.
[88] S. Barheine, S. Hayakawa, A. Osaka, C. Jaeger, Chem. Mater. 21 (2009) 3102.
[89] M.J. Duer, T. Friscic, R.C. Murray, D.G. Ried, E.R. Wise, Biophys. J. 96 (2009) 3372.
[90] S. Maltsev, M.J. Duer, R.C. Murray, C. Jaeger, J. Mater. Sci. 42 (2007) 8804.
[91] J.H. Zhan, Y.H. Tseng, J.C.C. Chan, C.Y. Mou, Ad. Func. Mater. 15 (2005) 2005.
[92] Y.-H. Tseng, C.Y. Mou, J.C.C. Chan, J. Am. Chem. Soc. 128 (2006) 6909.
[93] D. Laurencin, A. Wong, W. Chrzanowski, J.C. Knowles, D. Qiu, D.M. Pickup, R.J. Newport, Z. Gan, M.J. Duer, M.E. Smith, Phys. Chem. Chem. Phys. 12 (2010) 1081.
[94] Y.H. Tseng, Y.L. Tsai, T.W.T. Tsai, J.C.H. Chao, C.P. Lin, S.H. Huang, C.Y. Mou, J.C.C. Chan, Chem. Mater. 19 (2007) 6088.
[95] N. Dajda, J.M. Dixon, M.E. Smith, N. Carthey, P.T. Bishop, Phys. Rev. B 67 (2003) 024201.
[96] J.F. Stebbins, K.E. Kelsey, Phys. Chem. Chem. Phys. 11 (2009) 6906.
[97] L.S. Cahill, S.-C. Yin, A. Samoson, I. Heinmaa, L.F. Nazar, G.R. Goward, Chem. Mater. 17 (2005) 6560.
[98] J. Cabana, J. Shirakawa, G. Chen, T.J. Richardson, C.P. Grey, Chem. Mater. 22 (2010) 1249.
[99] L.S. Cahill, C.W. Kirby, G.R. Goward, J. Phys. Chem. C 112 (2008) 2215.
[100] J.L. Herberg, R.S. Maxwell, E.H. Majzoub, J. Alloys Comp. 417 (2006) 39.
[101] M.H.W. Verkuijlen, P.J.M. van Bentum, E.R.H. van Eck, W. Lohstroh, M. Fichtner, A.P.M. Kentgens, J. Phys. Chem. C 113 (2009) 15467.
[102] M. Jiang, B. Key, Y.S. Meng, C.P. Grey, Chem. Mater. 21 (2009) 2733.
[103] D. Zeng, J. Cabana, W.-S. Yoon, C.P. Grey, Chem. Mater. 22 (2010) 1209.
[104] Y. Makimura, L.S. Cahill, Y. Iriyama, G.R Goward, L.F. Nazar, Chem. Mater. 20 (2008) 4240.
[105] L.J.M. Davis, I. Heinmaa, G.R. Goward, Chem. Mater. 22 (2010) 769.
[106] B. Key, R. Bhattacharyya, M. Morcrette, V. Seznéc, J.-M. Tarascon, C.P. Grey, J. Am. Chem. Soc. 131 (2009) 9239.

An elegant study that demonstrates that in situ work is essential to really understand lithium incorporation in silicon battery electrodes.

[107] J.E.H. Sansom, J.R. Tolchard, M.S. Islam, D. Apperley, P.R. Slater, J. Mater. Chem. 16 (2006) 1410.
[108] A. Soleilhavoup, M.R. Hampson, S.J. Clark, J.S.O. Evans, P. Hodgkinson, Mag. Res. Chem. 45 (2007) S144.
[109] L. Holmes, L. Peng, I. Heinmaa, L.A. O'Dell, M.E. Smith, R.-N. Vannier, C.P. Grey, Chem. Mater. 20 (2008) 3638.
[110] P. Guerry, M.E. Smith, S.P. Brown, J. Am. Chem. Soc. 131 (2009) 11861.
[111] D. Raskar, M.T. Rinke, H. Eckert, J. Chem. Phys. C 112 (2008), 12530.
[112] L. van Wüllen, G. Tricot, S. Wegner, Solid State Nucl. Magn. Reson. 32 (2007) 44.
[113] E. Ratai, J.C.C. Chan, H. Eckert, Phys. Chem. Chem. Phys. 4 (2002) 3198.
[114] P. Florian, F. Fayon, D. Massiot, J. Chem. Phys. C 113 (2009) 2562.

[115] J. Hiet, M. Deschamps, N. Pellerin, F. Fayon, D. Massiot, Phys. Chem. Chem. Phys. 11 (2009) 6935.
[116] S.K. Lee, M. Deschamps, J. Hiet, D. Massiot, S.Y. Park, J. Phys. Phys. B 113 (2009) 5162.
[117] T. Charpentier, S. Ispas, M. Profeta, F. Mauri, C.J. Pickard, J. Phys. Phys. B 108 (2004) 4147.
[118] T. Charpentier, P. Kroll, F. Mauri, J. Phys. Phys. C 113 (2009) 7917.
An illustration of the significant progress that has been made to combine first principles DFT calculations with NMR in a glass to provide real new structural insight.

Figure Captions

Figure 1. The use of variable magnetic fields to constrain simulations of NMR spectra by comparing with experimental data collected at several magnetic fields illustrated by (a) ^{25}Mg in $MgSO_6.6H_2O$ at three magnetic fields showing the two inequivalent magnesium sites, and (b) ^{93}Nb from $YNbO_4$ at four magnetic fields. Reproduced from [9] and [10] respectively with permission of the copyright owner.

Figure 2. ^{27}Al static NMR powdered α-Al_2O_3 using a 300 μm microcoil (black line) using a spin-echo compared with the theoretical spectrum (gray line). Reproduced from [13] with permission of the copyright holder.

Figure 3. (a) ^{17}O DOR NMR at 14.1 T of L-alanine (in zwitterionic form) recorded with 30 kHz CW decoupling and sideband suppression with outer rotation at 1805 Hz. The simulated spectra (b) excluding and (c) including CSA show that its inclusion is necessary. Reproduced from [16] with permission of the copyright holder.

Figure 4. (a) Rotor assisted population transfer, (b) QCPMG pulse sequences which can be combined and (c) the effect on enhancing the signal of ^{33}S in a silicate glass using RAPT, QCPMG and RAPT-QCPMG.

Figure 5. (a) The refocused INADEQUATE NMR pulse sequence and (b) the ^{31}P INADEQUATE spectrum from a multiphase ceramic formed from a crystallised sodium calcium phosphate glass showing the three separate chain phosphate connectivities. Reproduced from [35] with permission of the copyright holder.

Figure 6. ^{71}Ga MAS NMR spectra of sol-gel formed β-Ga_2O_3 annealed at 1200 ^{o}C and then ball milled for 30 hours. Experimental data is shown for (a) ball milled and (c) annealed samples, along with the corresponding simulations (b) and (d) respectively, using the same χ_Q, but with a five times greater distribution for the ball milled sample (see text). Reproduced from [44] with permission of the copyright holder.

Figure 7. ^{95}Mo MAS NMR spectra of (a) $CdMoO_4$, (b) $PbMoO_4$ and (c) $CaMoO_4$ comparing the spectra at 11.75 and 21.14 T, reproduced from [60] with permission of the copyright owner, and (d) α-$ZnMoO_4$ showing the three distinct molybdenum sites reproduced from [61] with permission of the copyright owner.

Figure 8. (a) Natural abundance ^{43}Ca MAS NMR REDOR spectra from hydroxyapatite, allowing the distinction of the two sites on the basis of the differential proton coupling and (b) ^{1}H{^{43}Ca} R^3-HMQC of hydroxyapatite and oxyhydroxyapatite showing the increase in inequivalent sites as

defects are introduced in the oxyhydroxyapatite reproduced from [72] with permission of the copyright owner.

Figure 9. Wideline ^{10}B NMR spectra showing the approach of individual field-step components (a), and for a $Cs_2O.9B_2O_3$ the ^{10}B spectrum (b) with the BO_3 and BO_4 signals arising from the boroxyl and triborate structural units present.

Figure 10. ^{31}P MAS-J-INADEQUATE spectrum of β-$Ca(PO_3)_2$ showing the connectivity of the PO_4 units reproduced from [83] with permission of the copyright owner.

Figure 11. ^{31}P MAS NMR spectra for $Li_3V_2(PO_4)_3$ showing the effect of different spinning speeds, with spinning sidebands marked by asterisks, reproduced from [99] with permission of the copyright owner.

Figure 12. (a) A one-pulse ^{31}P MAS NMR spectrum of a cadmium phosphate glass (with the chemical shift scale given by the single quantum axis of the 2D INADEQUATE spectrum below in (c)) with different (b) P_n groups whose relative proportions depend on the glass composition. (c) A 2D refocused INADEQUATE spectrum (in pseudo-COSY SQ-SQ representation) reveals the connectivity of P_n groups and (d) a 2D z-filtered spectrum partially resolves the $^2JP;P$-coupling constants reproduced from [110] with permission of the copyright owner. (e) ^{27}Al DQ MAS NMR spectrum of a magnesium aluminoborate glass revealing the correlations between the different AlO_x units and the empty squares indicating where other possible correlations should have been if they were present in the sample reproduced from [116] with permission of the copyright owner.

Figures

Figure 1

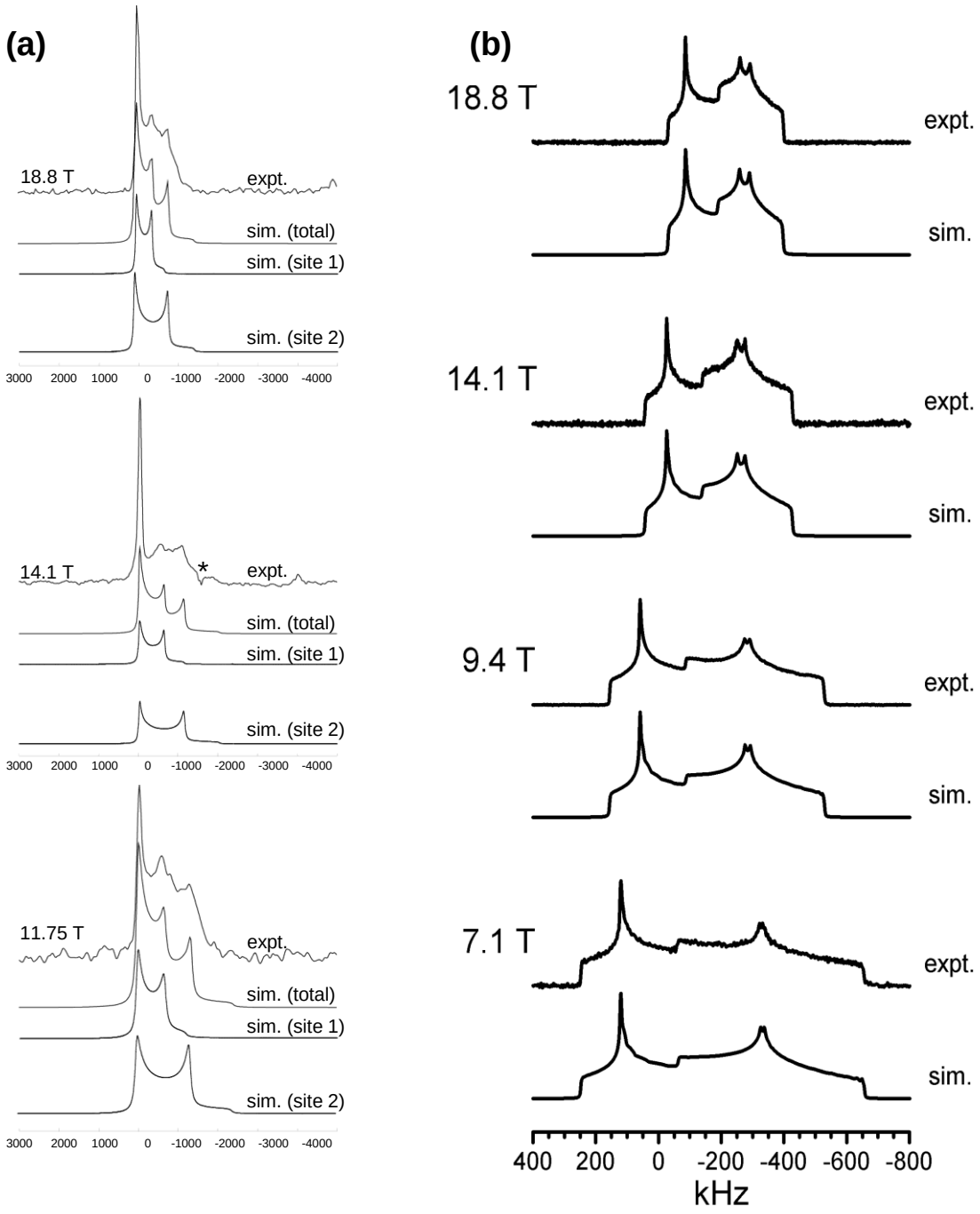

Figure 2

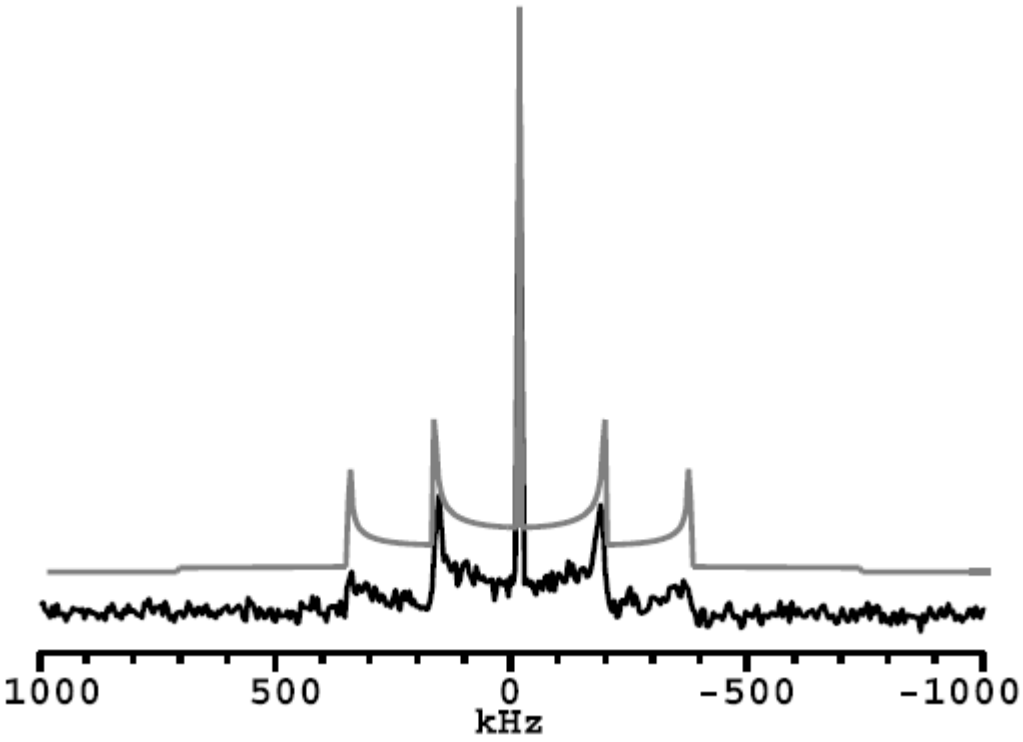

Figure 3

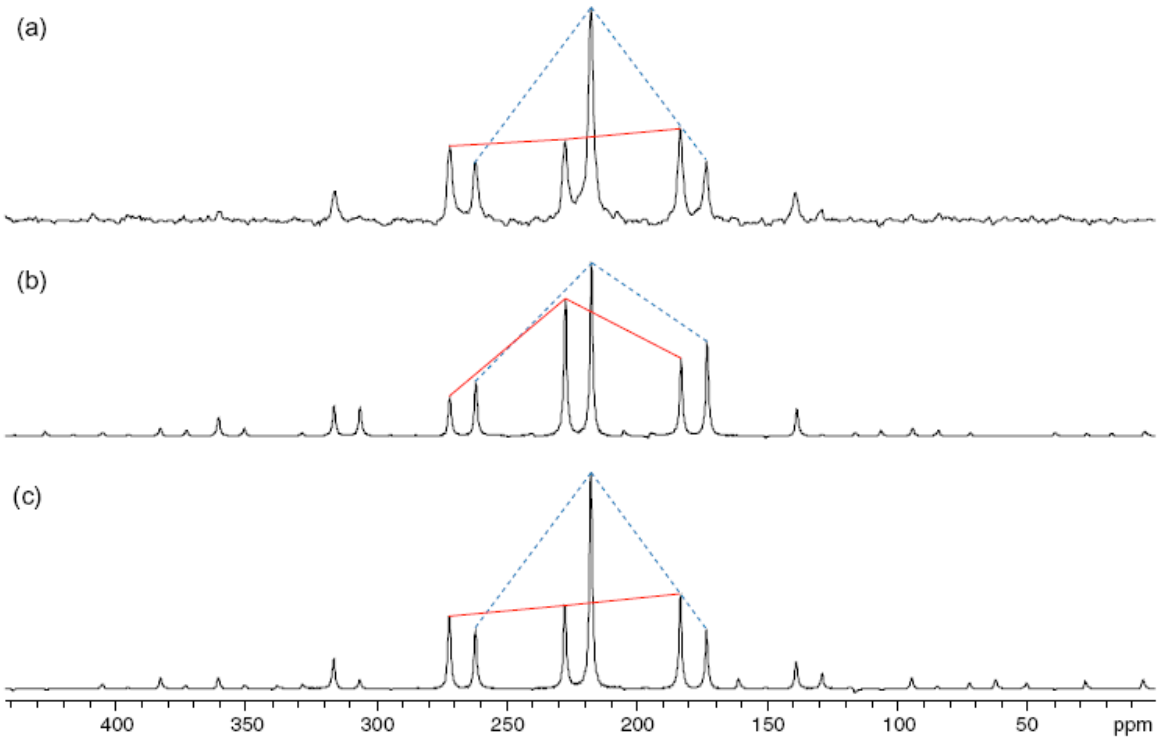

Figure 4

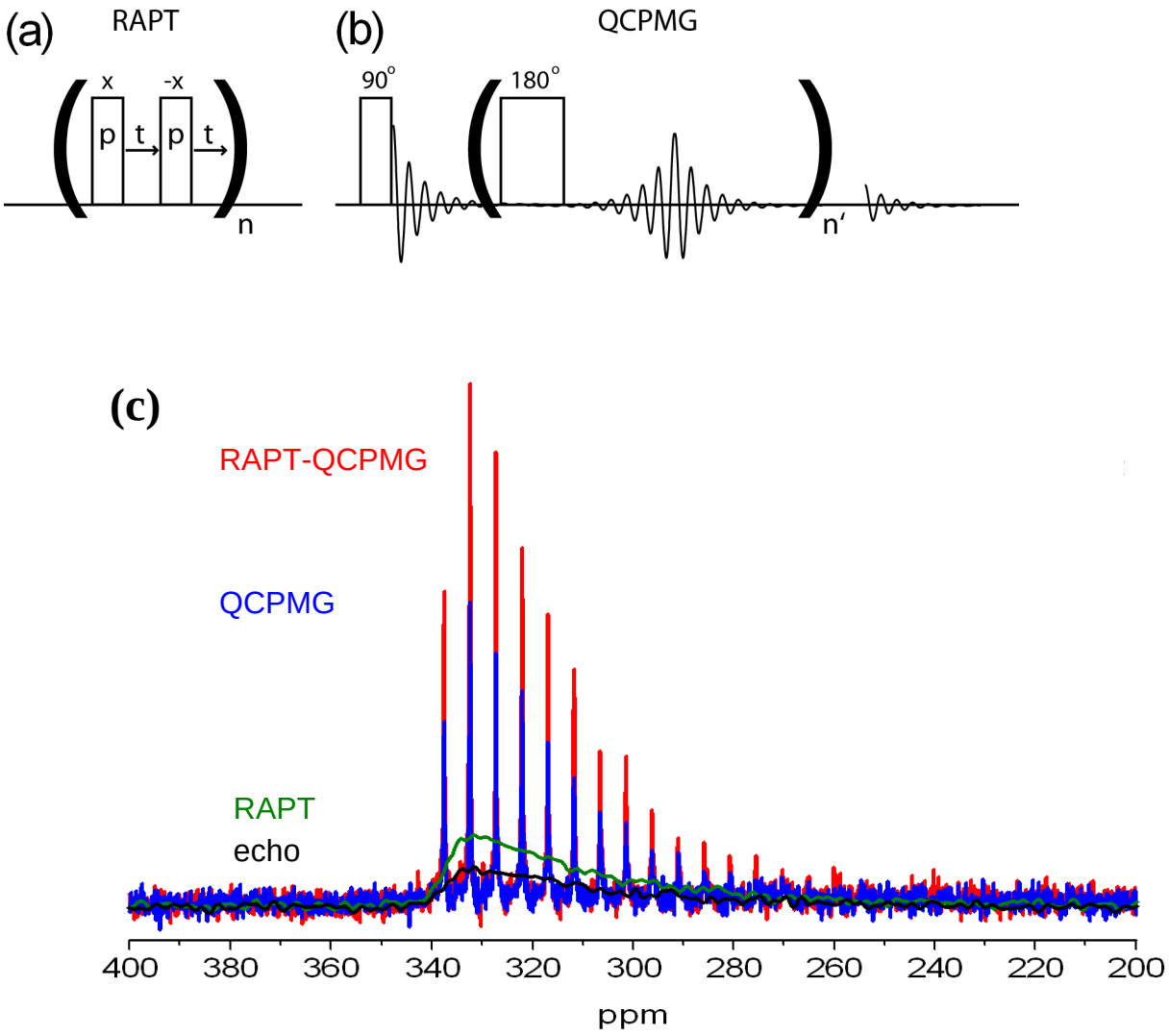
(a)
RAPT
x
-x
p
t
p
t
n
(b)
QCPMG
90°
180°
n′
(c)
RAPT-QCPMG
QCPMG
RAPT
echo
400
380
360
340
320
300
280
260
240
220
200
ppm

Figure 5

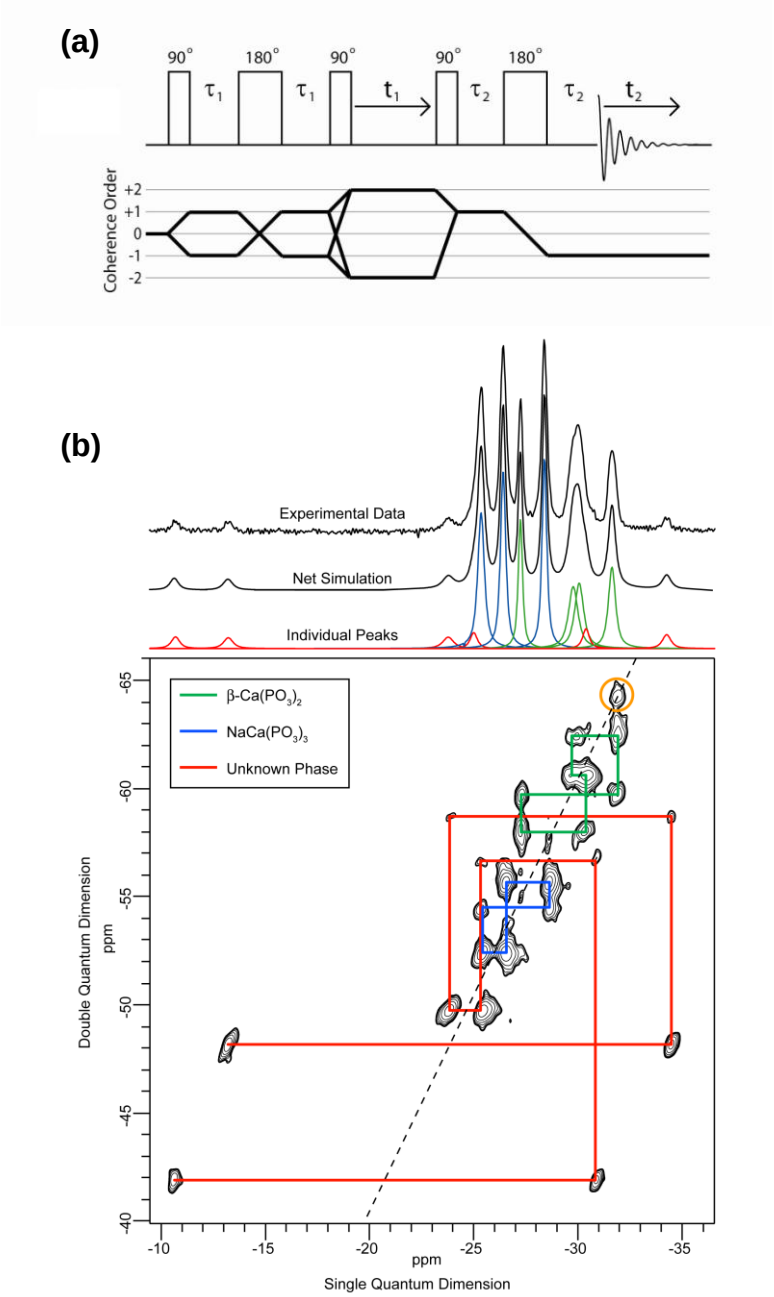
(a)
90°
180°
90°
90°
180°
τ1
τ1
t1
τ2
τ2
t2
Coherence Order
+2
+1
0
-1
-2
(b)
Experimental Data
Net Simulation
Individual Peaks
β-Ca(PO3)2
NaCa(PO3)3
Unknown Phase
Double Quantum Dimension
ppm
-65
-60
-55
-50
-45
-40
-10
-15
-20
-25
-30
-35
ppm
Single Quantum Dimension

Figure 6

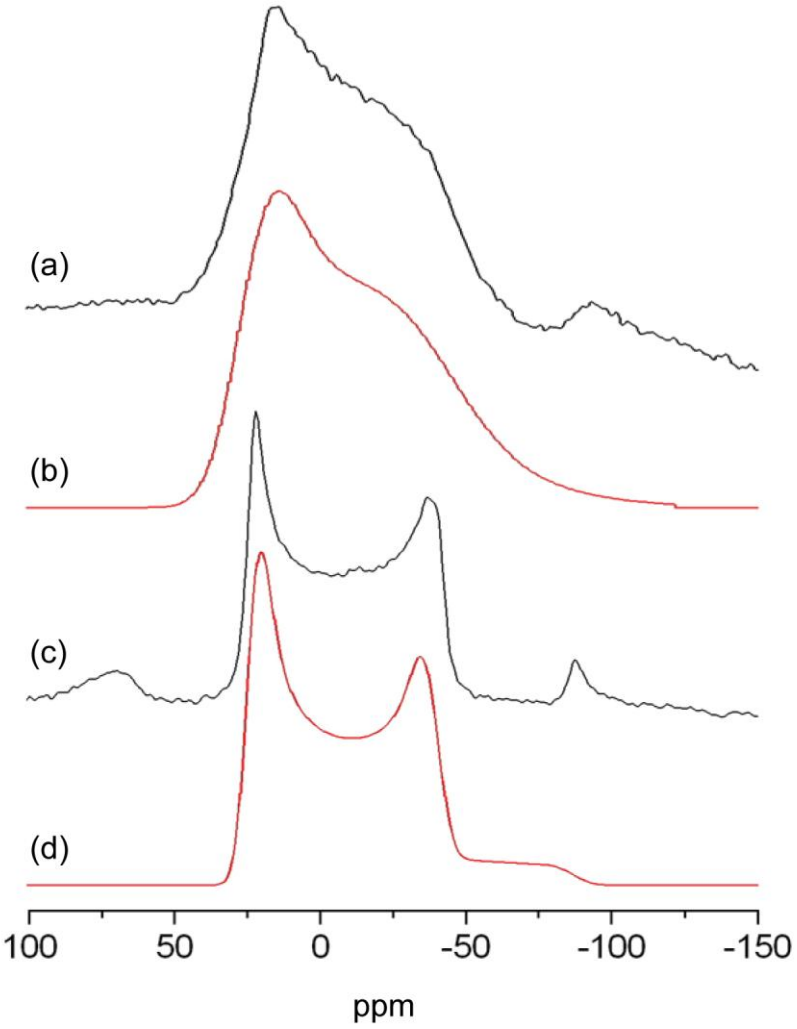

Figure 7

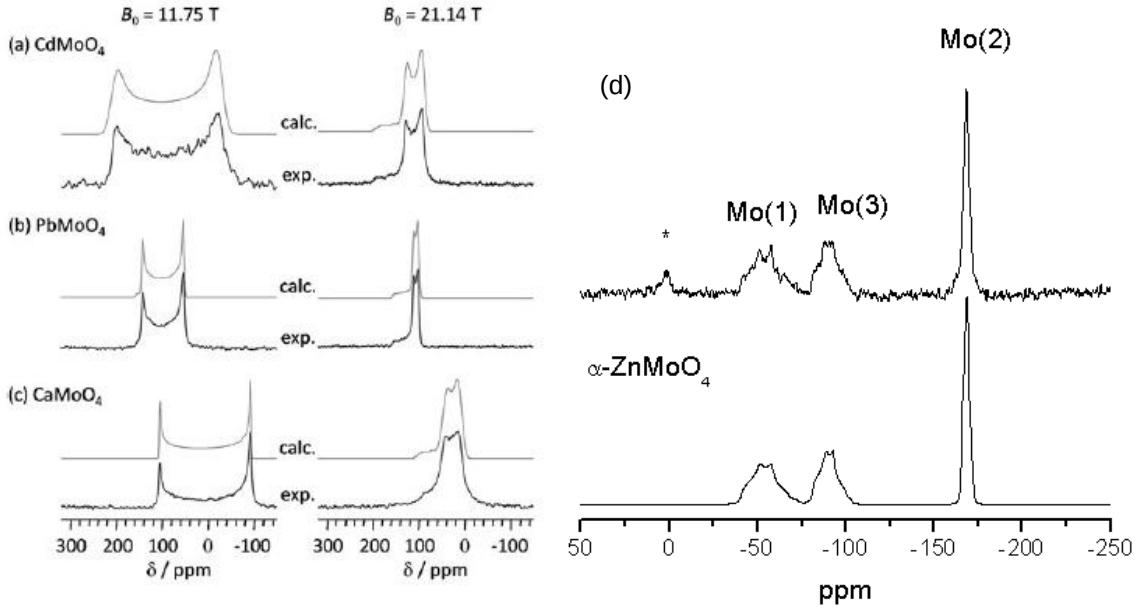
B_0 = 11.75 T
B_0 = 21.14 T
(a) $CdMoO_4$
(b) $PbMoO_4$
(c) $CaMoO_4$
calc.
exp.
300 200 100 0 -100
δ / ppm
(d)
Mo(2)
Mo(1)
Mo(3)
*
α-$ZnMoO_4$
50 0 -50 -100 -150 -200 -250
ppm

Figure 8

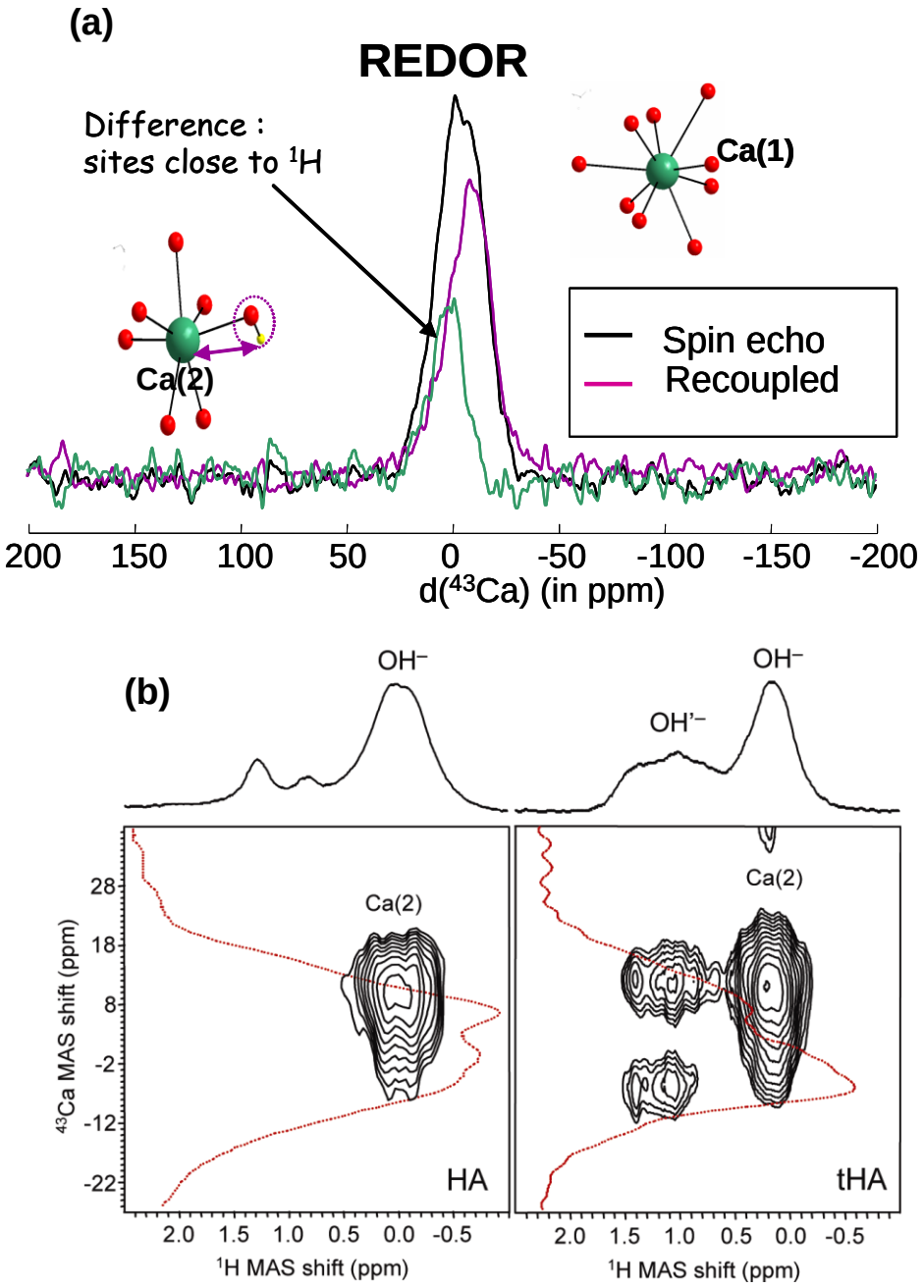
(a)
REDOR
Difference :
sites close to ¹H
Ca(1)
Ca(2)
Spin echo
Recoupled
200 150 100 50 0 -50 -100 -150 -200
d(⁴³Ca) (in ppm)
(b)
OH⁻
OH'⁻
OH⁻
Ca(2)
Ca(2)
⁴³Ca MAS shift (ppm)
28
18
8
-2
-12
-22
HA
tHA
2.0 1.5 1.0 0.5 0.0 -0.5
¹H MAS shift (ppm)
2.0 1.5 1.0 0.5 0.0 -0.5
¹H MAS shift (ppm)

Figure 9

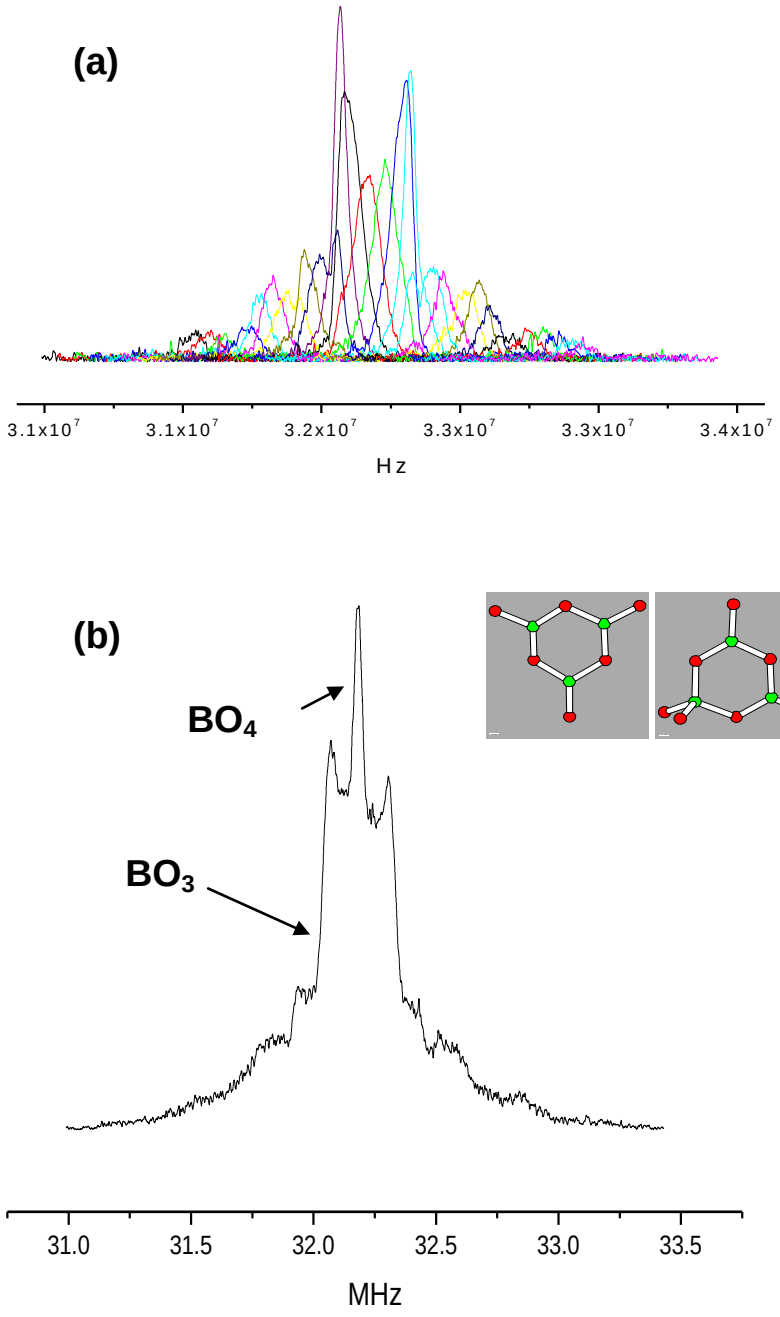
(a)
3.1x10^7
3.1x10^7
3.2x10^7
3.3x10^7
3.3x10^7
3.4x10^7
Hz
(b)
BO4
BO3
31.0
31.5
32.0
32.5
33.0
33.5
MHz

Figure 10

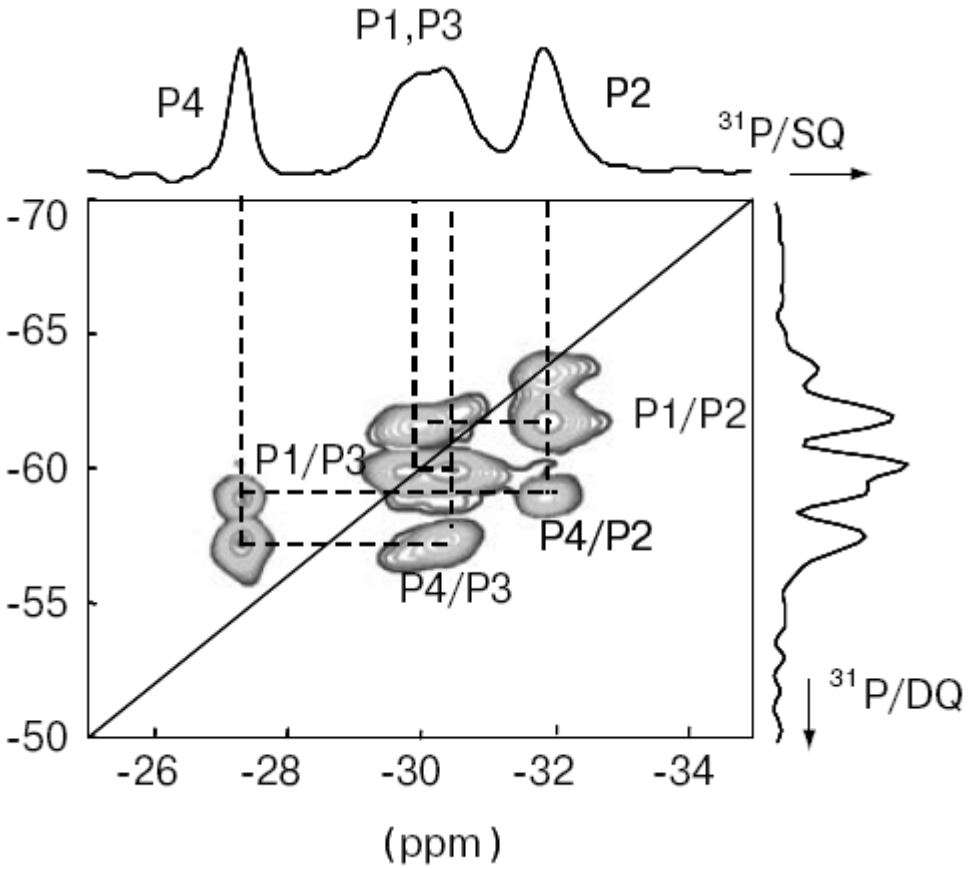

Figure 11.

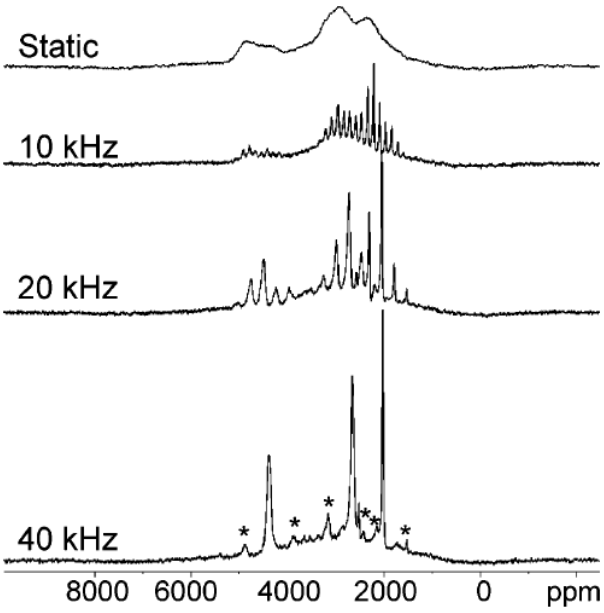

Figure 12

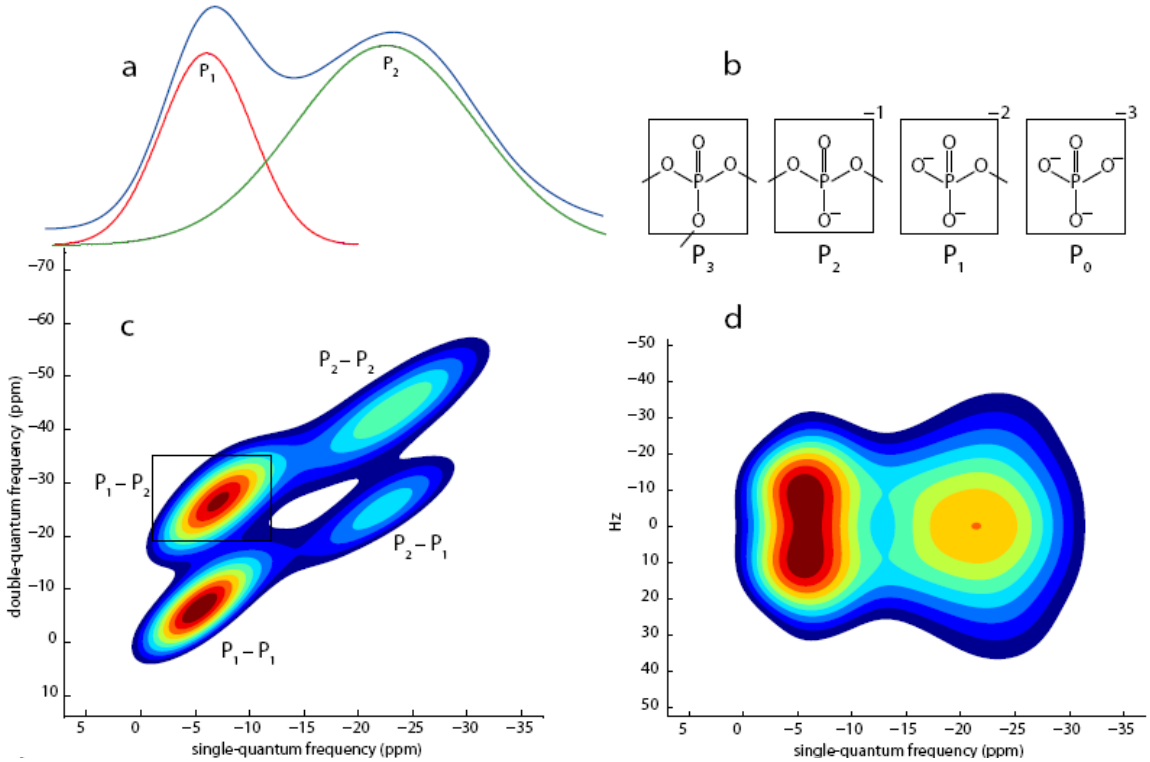
a
P1
P2
b
−1
−2
−3
P3
P2
P1
P0
c
P2 – P2
P1 – P2
P2 – P1
P1 – P1
double-quantum frequency (ppm)
single-quantum frequency (ppm)
d
Hz
single-quantum frequency (ppm)

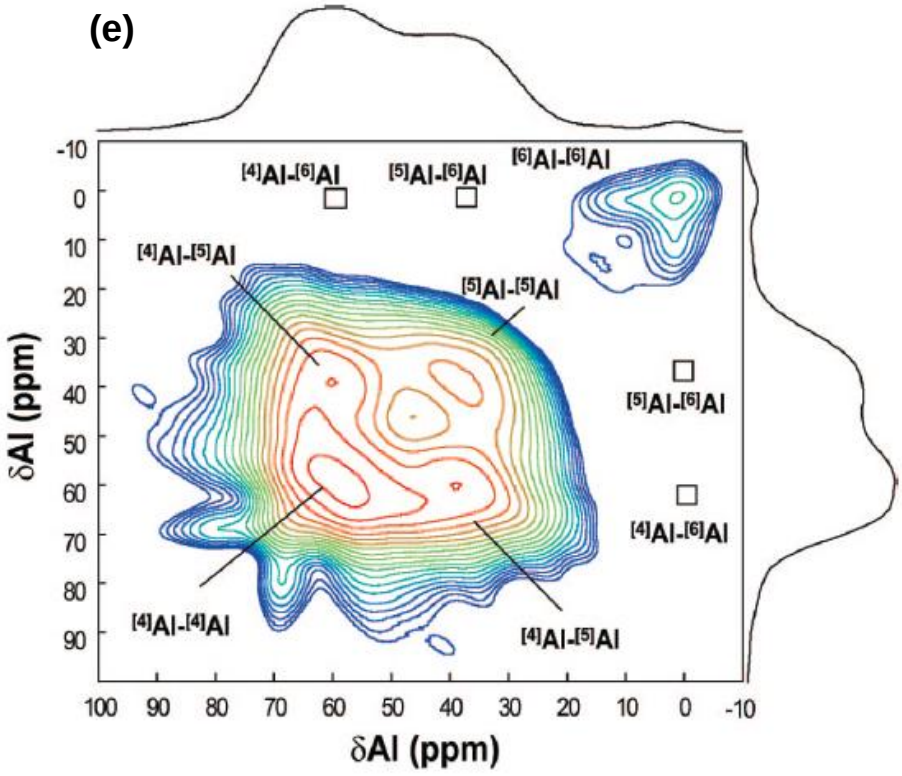
(e)
[4]Al-[6]Al
[5]Al-[6]Al
[6]Al-[6]Al
[4]Al-[5]Al
[5]Al-[5]Al
[5]Al-[6]Al
[4]Al-[6]Al
[4]Al-[4]Al
[4]Al-[5]Al
δAl (ppm)
δAl (ppm)